LUMINESCENCE STUDIES OF TRACE GASES THROUGH METASTABLE TRANSFER IN COLD HELIUM JETS

A Dissertation

by

SCOTT COLTON WILDE

Submitted to the Office of Graduate and Professional Studies of
Texas A&M University
in partial fulfillment of the requirements for the degree of

DOCTOR OF PHILOSOPHY

Chair of Committee, David M. Lee
Committee Members, Marlan O. Scully
Alexey A. Belyanin
Valery L. Pokrovsky
Haiyan Wang
Department Head, George R. Welch

May 2016

Major Subject: Physics

ABSTRACT

Among the elements, Helium has the largest steps among its internal energy structure that can keep for long periods of time, hence the metastable helium moniker. It is referred to as a “nano-grenade” in some circles because of how much energy it can deliver to a space roughly the size of an atom. This work demonstrates a method to create metastable helium abundantly and it is used to excite trace amounts of oxygen to the point where the signal received from the oxygen was larger than the signal received from the helium in a cold atomized jet. Further cooling of the jet and turbulence added by a liquid helium surface worked to increase the oxygen signal and decrease the helium signal. This work investigates the possibility of forming a strong metastable helium source from a flowing helium gas jet excited by passing through ring electrodes introduced into a cryogenic environment using evaporated helium as a buffer gas.

Prior study of luminescence from trace gases at cold helium temperatures is virtually absent and so it is the motivation for this work to blaze the trail in this subject. The absence of ionic oxygen spectral lines from the transfer of energy that was well over the first ionization potential of oxygen made for a deeper understanding of collision dynamics with multiple collision partners. This opened the possibility of using the high energy states of oxygen after metastable transfer as a lasing transition previously unavailable and a preliminary analysis

suggested that the threshold for lasing action should be easily overcome if feedback were introduced by an optical cavity.

To better understand the thermodynamics of the jet it was proposed to use diatomic nitrogen as an in situ thermometer, investigating whether the rotational degrees of freedom of the nitrogen molecule were in thermal equilibrium with the surrounding environment. If the gas was truly in thermodynamic equilibrium then the temperature given by the method of using collisions of a buffer gas and the rotational temperature determined spectroscopically should be in agreement. It was found that metastable transfer from helium in the jet provides enough energy to create a population of hot molecules of nitrogen that never reach thermal equilibrium with the buffer gas which is almost entirely made up of ground state helium atoms. This effect can be corrected for by adding some significant changes to the optical setup but are not outside the realm of possibility as they have been designed and built for other experiments. Therefore the rotational spectra of nitrogen could be used as an in situ thermometer at cryogenic temperatures with metastable helium present provided the hot molecule contribution due to collisions of the second kind of nitrogen and helium is measured and removed.

To my parents and my family,

to my wife that I will forever love,

and to everyone who has helped me without my knowing.

ACKNOWLEDGEMENTS

First and foremost, this dissertation could not have come to be without the help and support of my advisor, Dr. David M. Lee, who always went out of his way to make sure that I was on track to finishing and keeping my thoughts organized. I could not imagine a better boss that would be more understanding or more thoughtful and helpful. Even during the roughest times he made everything bearable, it was always a delight to speak with him, and I'm sure he did many things behind the scenes to help me that I probably will never know about. I doubt I will ever have a better mentor and friend that could match what he has been for me. No matter what was going on he always seemed to be in a contagiously positive mood. Also I would like to thank the rest of the group in the low temperature physics laboratory, Vladimir Khmelenko, Patrick McColgan, Adil Meraki, Shun Mao, and Trevor Dragon, without their work and heavy lifting this dissertation would have been impossible.

There was the insight and input from faculty members at Texas A&M University Department of Physics and Astronomy, particularly the many discussions I had with Dr. Hans Schuessler, who may never know how much he helped me through his comments and suggestions. It was always a pleasure to learn from Drs. Aleksei Zheltikov and Artem Abanov, who both taught me statistical and quantum physics so well that I should be able to do it in my sleep, and Dr. Andrew Weimer taught me the importance of appreciating the history of

physics and the development of theoretical frameworks. I will never forget the many lessons I learned from Drs. Christopher Pope and Bhaskar Dutta, both of whom made me appreciate and understand astrophysics at a level I never dreamed I would be able to. Members of other departments at Texas A&M University have also been an inspiration and a source of knowledge such as Drs. Philip Hemmer, Simon North, and many others from the Cyclotron Institute who gave me the pleasure and opportunity to work on some of their experiments for fun. There are conversations and lectures that had inspired me from many other faculty members, and they may never know how much they had inspired me and are too many to list here. Also I would like to thank the members of my committee, Marlan Scully was very patient and supportive of me at the beginning of my time here at this university and I had the wonderful opportunity to join his group at the Institute for Quantum Science and Engineering. Valery Pokrovsky became a wonderful friend and without his patience I may not have ever passed his quantum mechanics course and it is to his credit that I so thoroughly understand scattering theory. I should also not forget to thank the rest of the committee members who I have been so lucky to have help me through this work, Drs. Alexei Belyanin and Haiyan Wang. The office staff at the department of physics deserves a mention here, specifically Minnette Bilbo, Veronica Rodriguez, Sherree Kessler, Jill Lyster, Barbara Siems, Todd Hansen, and everyone else that works in the department office who endured much to make sure that I was able to finish this work and provide for the success of the

experiment. I would like to mention my masters advisor, Dr. David Shelton, from University of Nevada, Las Vegas, who helped me review some of the laser calculations in this work. I would also like to thank all of the people in Bryan and College Station who I have made friends with over the time I've been here that helped me in many ways to survive without losing my sanity, specifically Hank Seidel, Glenn Pruitt, Autumn Deschaines, Mitch Wood, Timothy Campbell, and Steven Johnson. I would like to also thank all the people from Patterson Architects, Sweet Eugene's House Of Java, The Farm Patch Market, Outkasts Car Club of Texas, Dolliver Enterprises, Texas Aggieland Brew Club, the "Shire of the Shadowlands" branch of the Society for Creative Anachronism, and Carney's Pub. I could not express enough thanks for the slurpee machine that magically appeared in town and even in a store that wasn't a 7-11.

Last but not least I would like to thank my family for having the patience and loving support that they gave me. I believe I could not have been able to do anything that I have done without them. Specifically I would like to thank my wife, Jill Geary, whom waited for four years to join me in Texas while waiting for her visa. I don't believe I could have survived any of this without her support and patience throughout all that time.

TABLE OF CONTENTS

LIST OF FIGURES

1. INTRODUCTION

Finding pathways to generate large populations of metastable helium and understanding the possible interactions through processes at several different temperatures is a fairly large and ambitious project to undertake. This work sets out to describe metastable transfer with trace gases, more specifically with atomic oxygen and molecular nitrogen, by studying luminescence from such processes. Once the processes are understood, a method of producing lasing action from a medium similar to the one under study in this work is proposed.

1.1 Early history

The importance of the transfer of energy from metastable helium to atoms and molecules through the process of metastable transfer has been put forward by many studies. Research over many pressures and mixture ratios in both stationary and flowing gas have provided some understanding of the role of metastable helium in the luminescence measured from different trace elements. However, there were not many studies of metastable transfer in cryogenic environments in the early days, and to find work that measured luminescence below the boiling point of liquid nitrogen is almost impossible. Therefore a study of this phenomenon at cryogenic temperatures should be undertaken to increase the understanding of the luminescence processes.

Helium is probably the simplest atom to study and the wave functions for the two electron system are well known and can be calculated exactly. This

makes it viable for many kinds of research involving high precision measurements and also checking theoretical predictions from all over the gamut, starting in atomic physics and ending in quantum chemistry. ^{4}He is the most abundant isotope of helium which is naturally found in the atmosphere. It has no nuclear spin and therefore has no hyperfine structure, which lends itself to simplicity. Spectroscopy of high accuracy of the electronic energy levels provided for tests of quantum electrodynamics and a value of the fine structure constant.

This work is an extension of previous studies of nanoclusters with trapped impurities injected into He II [1]. After the advent of stable high frequency radio discharges, glows and afterglows could be prepared with electrodes outside the medium under study behind dielectric barriers such as quartz which provided protection to the electrodes and also lowered the possibility of vaporization from the surface of the electrodes introducing contaminants to the sample under study [2]. Dielectric barrier discharges provide ideal control parameters for establishing non-equilibrium plasma conditions in a controllable way. Colder temperatures of gas flow discharges could then be studied by immersing the barrier and electrodes in cryogenic environments thereby providing greater insight into the diverse dynamics of charge recombination and energy transfer of atoms and molecules. A jet of helium vapor with trace gases flowing through a quartz tube can be made to discharge through ring electrodes, provided the density allows breakdown, and can thus atomize molecules in the sample. Low

densities of atomic impurities inside large densities of helium can remain separated for large amounts of time as the gas flows beyond the discharge. Forming this jet allows for nanoclusters of impurities to form in the jet through Van Der Waals forces between slow moving molecules. As the density of impurities is decreased, the cluster density decreases and at very low densities the clusterization effect is avoided entirely during the passage of the jet. By avoiding clusterization one can study the interaction of slow moving molecules and atoms in the jet of helium. The method presented in this work generates excited states in impurities and helium that are co-moving on the same axis with negligible relative velocities which allows for studying energy transfer between them. This work only provides a narrow slit down the side of glass dewars for optical access, and so the intensity due to reflections off the walls of each cryostat can probably only be known to a few orders of magnitude estimate. Still, studies of spectral emission due to metastable transfer from helium at low temperatures are few and far between and this work intends to pioneer the research needed to understand these processes.

The nature of light was first described by Maxwell [3] in his work developing the classical theory of electromagnetic radiation that married electricity, magnetism, and light as conceptually of the same origins [4]. It was later when Max Planck [5] published his famous result in 1900 that introduced his famous postulate that electromagnetic energy could only be emitted in quantized forms, or what would later be referred to as photons. Without these

previous studies the concept of “light amplification by stimulated emission of radiation” or LASER for short would not have come about. Einstein developed the theory for stimulated emission in 1916 [6], following which came Rudolf Ladenburg who in 1928 [7] confirmed that stimulated emission and the concept of negative absorption should exist. The term “photon” was accidentally introduced by Gilbert Lewis in 1926 [8] that ended up being used as the name for what Einstein had referred to as “light quanta” in his work describing the nature of light. It was an accident because the quantity that Lewis intended to introduce and emphasize in his publication was the number of photons and not the term photon itself. The idea of population inversion was put forward by Valentin Fabrikant in 1940 and about that time many scientists and engineers started looking for suitable media to create a laser device. One interesting and little known fact is that while all of this was happening there was a group studying spectral emission from low density xenon discharges. This group that was spearheaded by Curtis J. Humphreys [9] would have been the first to claim operation of a gas laser if they had been using photodetectors sensitive in the mid-infrared. Xenon has unusually strong emissivity values for two atomic lines in the mid-infrared, specifically 2.1 and 3.5 μm, so that even in short laser tubes with no mirrors will exhibit laser oscillation.

For the gas phase lasers that would be later developed, Maxwell enters the scene again with his heuristic derivation of what is now known as the Maxwell-Boltzmann distribution [10]. This distribution was used to introduce the

concept of what becomes later known as the “Boltzmann factor” which gives the ratio of populations for definite states and at a given temperature [11]. Statistical mechanics tells us that when a large collection of similar atoms are in thermal equilibrium the relative populations of any two energy levels are related by this factor [12]. When the energy difference between the states is much larger than the thermal energy at equilibrium, kT, the ratio of populations tends to zero and there will be few atoms in the upper energy level as compared to the lower level when the system is thermalized. This leads to the prediction that at absolute zero, all the atoms will be in the ground state. It also leads to the prediction that at thermal equilibrium a state with a lower energy must always be more densely populated than a state with higher energy which means optical amplification is not possible while in thermal equilibrium.

In 1947, Lamb [13] shows experimental evidence of induced emission in hydrogen spectra. Charles H. Townes would later invent the MASER, corresponding to microwave amplification of stimulated emission of radiation, the theory for which he wrote down while sitting on a park bench on a scrap piece of paper while waiting for a restaurant to open for breakfast before attending an Office of Naval Research conference on millimeter wave generation. Townes proposed to build a device based on this theory to his postdoctoral and graduate student that later took them until 1953 to demonstrate amplification and later continuous amplification [14]. This would turn out to be the first device on the scene that used stimulated emission. In the same year there were two other

inventors that produced a MASER in Moscow's Lebedev Institute of Physics, Alexander Prokhorov and Nikolai G. Basov, who had found MASER oscillation while they were searching for quantum oscillators in gaseous media [15]. The history continues through many notable contributions by several people but the concept of light amplification in a resonant cavity all started in 1940 and continued until Maiman demonstrated pulsed lasing in a ruby crystal in 1960 [16]. Seven months later the helium-neon laser developed by scientists at Bell laboratories demonstrated a continuous beam instead of pulses through a steady population inversion as discussed below [17].

Previous to the helium-neon laser there had been several years of gas spectroscopy experiments that generated huge tables of spectral lines that were used in the search for proper candidates for gas phase lasing media. Two mechanisms were identified for proper production of population inversions in gases, optical pumping and excitation through electron impact, or what can be called discharge excitation. The efficiency and the complications of optical pumping turned out to be detrimental for generating large population inversions in gas phase media as opposed to direct excitation through electron impact. The first major research that started examining discharge pumping was done by Ali Javan who had proposed using the concept of "collisions of the second kind" to excite neon from helium that was excited by electron impact and eventually built the first operational helium-neon laser in 1961 at Bell labs [17].

The concept of the operation of the helium-neon (HeNe) laser is simple and relies upon the concept of metastable transfer from helium atoms. A thin tube is filled with about 2 Torr of a helium and neon mixture with approximately 10% neon concentration. A discharge in the gas is established by a few kilovolts between electrodes in the gas. Electrons in the discharge collide with helium and excite the atoms to their long lived metastable 2S states that lie above the ground state by about 20 eV; two states in particular, one at 20.65eV and another at 19.8eV. What Javan had known and inferred was that these levels are about the same energy as the 4S (~19.8eV) and 5S (~20.6eV) levels of neon as compared to their ground state and that collisions with helium would deliver the energy to excite the neon to these levels. The 5S and 4S states decay to the 3P or 4P states with these wavelengths.

$$
\begin{aligned}
5S \rightarrow 3P, &\qquad \lambda = 632.8 \text{ and } 543 \text{ nm} \\
4S \rightarrow 3P, &\qquad \lambda = 1523 \text{ nm} \\
5S \rightarrow 4P, &\qquad \lambda = 3391 \text{ nm}
\end{aligned}
$$

The 3P level de-excites fast to the 3S state, and then the rate of return to the ground state is enhanced by collisions with the walls of the vessel. Most often in commercial applications the red line is selected out by using mirrors coated with an anti-reflection coating that rejects the other lines. There exists an empirical formula that relates the pressure (in Torr) to the tube diameter, namely pD~4 Torr-mm, which means usually the tube diameter should be on the order of millimeters in order to quickly de-excite to the lower laser state. As a result,

the optical cavity is usually 20-50cm long and the electrodes are also usually recessed out of the way of the optical path between the windows of the laser.

Not long after Javan and his colleagues had developed the HeNe laser Kumar Patel developed the CO_2 laser [18]. Gases of molecules provide the means for higher power and efficiencies than atomic gases because molecular electronic levels are closer to the ground state and therefore less energy is required to pump them to excited states. The carbon dioxide molecule also has energy levels coincident with molecular nitrogen, specifically the $N_2^*(v = 1)$ and the $CO_2(00^o1)$ vibrational levels. Through metastable transfer of the nitrogen long-lived state to the carbon dioxide molecule a much better efficiency can be obtained. The nitrogen molecular level is an abnormally low energy state but it is long-lived so it can be easily excited by electron impact and it can then transfer this energy to a carbon dioxide molecule through collisions. This process produces a high continuous wave laser power output in the 10-micron region of infrared.

1.2 Planck's law and spectral broadening

When electromagnetic radiation is trapped in a container or cavity that is in thermal equilibrium with the walls of the cavity, the distribution of the radiation density within a small bandwidth is given by Planck's law. One important factor that should be familiar to anyone with even a pedestrian knowledge of laser physics is contained in Planck's law which determines the density of modes per

unit volume and unit frequency interval. This factor should also be familiar to anyone who has studied statistical physics because it can be interpreted as the number of degrees of freedom associated with a radiation field per unit volume and per unit frequency interval [19]. The expression for the mode density, $\mu(v)$ which contains the square of the frequency, is part of the connection between the spontaneous and stimulated or induced emission transition probabilities.

$$u_{\mathrm{T}}(v) = \mu(v)\vartheta_{\mathrm{T}}(v)hv = \frac{8\pi v^2}{\mathrm{c}^3}\frac{hv}{e^{hv/\mathrm{kT}} - 1} \qquad [1]$$

The energy density, $u_{\mathrm{T}}(v)$, is proportional to the mode density and the number of photons per mode in thermal equilibrium which is given by the Bose-Einstein distribution which is well known to be the blackbody distribution first described by Planck [20]. This energy density equation holds even for radiation resulting from non-thermal equilibrium and also the modes that are confined to oscillate in optical resonators.

At this point it is worthwhile to digress for a moment to introduce Einstein's A and B coefficients [6] which he introduced in 1916 as mentioned previously. Einstein applied the new concepts introduced by Planck and Boltzmann of thermal equilibrium that the probability for spontaneous emission by a transition from a higher state 2 to a lower state 1, dW_s, is proportional to the probability of stimulated emission, dW_{21}, which depopulates the upper state.

$$
\begin{aligned}
dW_s &= A_{21}d\mathrm{t} \\
dW_{21} &= B_{21}u\,(v)d\mathrm{t} \\
\frac{A_{21}}{B_{21}} &= hv\,\mu(v) = \frac{8\pi v^3}{c^3} \\
\frac{dW_{21}}{dW_s} &= \frac{B_{21}u\,(v)}{A_{21}} = \vartheta\,(v)
\end{aligned}
\qquad [2]
$$

The proportionality $\frac{A_{21}}{B_{21}}$ is found by inspection of the rate equations and balancing them by using the concept that light comes in the form of discrete energy packets. Further considerations of detailed balance and the energy density equation allows for one to write the relationship between the coefficients A_{21} and B_{21}which ends up being the density of modes for a frequency v times the energy at that frequency. Using these relationships the ratio of the rate of stimulated emission that is responsible for laser oscillation and coherent amplification and spontaneous or incoherent emission is just the number of photons per mode. It is important to note that although these equations are derived by using the condition of thermal equilibrium and detailed balance they hold also in the case of non-thermal radiation and confined modes. This is important because the ratio of stimulated emission and spontaneous emission defines the break-even point that is one photon in a particular mode. The quality of light or the coherence of light is usually defined by using this ratio, $\vartheta\,(v) < 1$ for incoherent light (usually the case for thermal light except for carefully constructed exceptions), and $\vartheta\,(v) > 1$ for coherent laser light. Typically for optical frequencies ($v = 10^{14}\mathrm{Hz}$) and laser operating temperatures (T<$10^4\mathrm{K}$) at thermal equilibrium $\vartheta\,(v)$ << 1, which corresponds to a Bose-Einstein condition on the population of each mode.

Transitions that are seen in the lab usually do not have a narrow and precise energy difference. For most situations the transition may have originated with a narrow and precise energy for all atoms or molecules that are involved in the emission but the circumstances under which the light is collected in the lab will mitigate the sharpness of the transition. For example, an atom forced to remain motionless will have an emission spectrum of an almost infinitely narrow line, once the atom is no longer restrained the narrow and sharp line in the emission spectrum broadens.

The lineshape and linewidth of a transition is caused by processes related to the lifetime, collision time, or just pure translational energy of the atom or molecule. Solid materials have further considerations to deal with, such as thermal effects, dipolar interactions, or structural inhomogeneities. All broadening mechanisms are put into two groups, homogeneous and inhomogeneous broadening.

Homogeneous broadening is called that because every atom contributes to the broadening of the spectral line in the same way so that the effect of a signal applied to the medium will have the same effect on all the atoms and molecules within it. Stated another way, a strong enough signal applied within the linewidth of the transition will saturate the transition uniformly. Spontaneous emission has a radiative lifetime and the transition probability is directly affected by it through the uncertainty principle. However its contribution is vanishingly small compared to collisional or pressure broadening. Collisions of radiating

particles with one another interrupt the radiative process of either emission or absorption and instead of producing a nicely defined continuous wave train it will produce a truncated wave train. After collision the particle will resume its motion with an added random phase and the radiative process can be restarted but it has lost all memory of the previous phase of the radiation prior to the collision. The resulting lineshape will tend to lead to a Lorentzian distribution.

Inhomogeneous broadening mechanisms will change the center frequencies of the transitioning particles that will broaden the overall response but doesn't broaden the individual response. Different particles will have slightly difference resonance requirements even for the same transition. One such difference results from Doppler shifts due to translating particles in random directions within the medium. This type of broadening will result in an applied signal only interacting with particles whose shifted resonance conditions match up to the signal frequency. Thus the applied signal will not have the same effect on all atoms in the medium. If the applied signal is strong enough it will eventually slice out a part of the absorption curve and this is usually called "hole burning" because it leaves part of absorption curve unused which is like burning a hole in a log instead of consuming the whole thing. There are also other examples such as magnetic resonance imaging which takes advantage of the variations of the resonant frequency due to a magnetic field gradient for different locations in a material medium.

1.3 Light oscillator

An oscillator that can sustain non-zero field intensity without any input fields is the definition of an amplifier with feedback. A laser is essentially a light amplifier although a better description might be a light oscillator. The condition that must be met in order for laser oscillation to occur is that the gain due to stimulated emission must be greater than the losses due to scattering, absorption, and transmission. It creates a lower limit of the gain that is required to maintain oscillation that is referred to as threshold gain. The rate equations for populations of levels allow for an approximation of the gain per pass coefficient, or low signal gain coefficient, which is found by solving a simple first order differential equation whose solution is a family of curves defined by the coefficient to the length of the active region within the cavity. Obviously this simplification is based on the assumption that the gain throughout the medium is continuous. If the gain per pass is greater than one than there is lasing, otherwise if the gain per pass is less than one the losses outnumber the gains so the cavity doesn't sustain feedback. To first order this calculated gain for a single pass through the cavity should indicate if the active medium can supply enough feedback to create lasing within the cavity. The gain per pass depends on the number density of atoms in the higher state, n, and the wavelength of emission λ, the linewidth of the transition w, and the lifetime of spontaneous emission, τ, is written in equation 3, where g is the gain per pass coefficient in

units of inverse distance, l is the length of the active medium, and $G(l)$ is the total gain of one signal traversing the active medium.

$$g = \frac{n\lambda^2}{8\pi^2 w\tau}, G(l) = e^{(gl)} \quad [3]$$

In this work the number of oxygen atoms flowing down the jet was measured to be $3 \times 10^{14} s^{-1}$. Approximating for a $10\ mm^2$ cross sectional area of the jet, the measured time for the jet to flow from the orifice to the liquid helium surface, a distance of 2.5 cm, was given as 100 microseconds so that the average velocity of each atom is 250 m/s. This gives an average number density of oxygen atoms passing a $10\ mm^2$ cross sectional area of the beam as $1.2 \times 10^{17}\ m^{-3}$. For lifetime broadened lines, the lifetime given for the oxygen 543 nm transition is 259 ns which yields a natural linewidth of 0.6 MHz. Using these values, the gain per pass coefficient is $2.4\ mm^{-1}$ which for a length across the jet of 1mm would give a gain of 120 per pass. This is more than sufficient to sustain laser operation. Even if only 1% of the oxygen atoms were in the upper excited state there could still be feedback given by a closed optical resonator with this medium inside it. One point to consider is that this calculation is independent of the design details of the cavity but it does make a strong argument that this transition in oxygen due to metastable transfer from helium in the jet could be used as a lasing medium provided a suitable cavity is made.

There was some concern early in this work about if the mirrors of such a cavity would be able to withstand cryogenic temperatures without distortion that would prevent lasing. Mirrors can be made with substrates that, provided they are cooled slowly enough, will not deform significantly at cryogenic temperatures. This has been demonstrated by several works but one most popular is by the workers at LIGO that published their discovery of gravitational waves using sapphire mirrors [21] but even for metallic mirrors the cryogenics should not be a problem as shown by also many workers and translation stages operating at that temperature are available commercially. Because of the concern this work did not venture further than the back of the envelope calculation given above towards observing lasing action in the jet due to optical feedback provided by mirrors inside the cryogenic environment. This would require a new cryostat design but the state of the art is already well beyond this requirement.

1.4 Optical nano-grenades

Metastable helium atoms store the largest amount of energy as compared with any other atomic or molecular system. This energy is so different from any other particle that even single atoms can be detected and because of this significant study of quantum statistical properties of large systems can be tested. It wasn't until after Einstein demonstrated quantized light through the photoelectric effect [22] that the treatment of light as a wave and a particle could be realized by de Broglie [23]. De Broglie postulated that there is a relationship

between the center of mass momentum of a particle and Planck's constant, or sometimes referred to as the quantum of action, and this relationship establishes that matter can travel as a wave. It wasn't long after he made this postulate that matter waves for electrons were demonstrated in the lab [24]. However the use of atoms in a similar optical fashion took a long time to develop since the de Broglie wavelength of a helium atom is comparable to the size of the atom's electronic wavefunction which required sensitive instrumentation to detect their optical properties. It wasn't until 1929 that Otto Stern [25] and colleagues [26] demonstrated specular reflection of atoms from surfaces. Optics using atoms had to wait until the advent of the laser and also the technology in the microelectronics industry to produce nanostructures effective enough to diffract atoms. In the 1980s there was an abundance of activity in the field of atom optics [27] which made use of the wave-particle nature of matter. Fast forward to today and there have been developed the means necessary to diffract, beam split, and reflect atoms. These tools allow for atomic interferometry [28] which brings with it the ability to measure the same things that light interferometers are capable of measuring, for example angular rotation, and also the ability to measure fine changes in gravitational gradients and therefore gravitational waves which as mentioned previously were measured recently [29], [21]. New frontiers in atom optics extend the capabilities of many fields. As is the case with most phenomena, the source material or in this case the atoms used in the atom optics experiments are chosen because of their unique structure. Alkali metals

are used frequently because of the ease of production through oven sources and also the simple valence electron structure which leads to some easily accessible optical transitions. Hydrogen is the simplest atom often used to demonstrate atomic structure properties but for the most part is not useful in atomic optics experiments mainly because technology today lacks a continuous wave laser at the Lyman-alpha range with sufficient intensity to excite many atoms at once. Perhaps one could say the reason hydrogen is not useful in atom optics is because there does not exist a simpler atom than hydrogen. The rare gases also have this problem because of their short wavelength transitions in the deep vacuum ultraviolet that is outside the reaches of today's cw laser wavelengths. However, electron impact can populate high lying states that have forbidden transitions and therefore create long-lived highly energetic atoms, or what Baldwin refers to as optical "nano-grenades" [30] and access to the wavelengths necessary to perform atom optics with rare gases are similar to considering a highly excited atom's metastable state as the effective "ground state" from which existing lasers can access transitions from this state to other high lying states. Obviously the grenade part of "nano-grenades" is the large amount of energy that can be stored internally and for rare gas atoms this energy is largest, and specifically for helium, it is ~20eV. There also exists the advantage that when the metastable atom or molecule de-excites through wall collisions or with other molecules it has essentially disappeared with the lost energy; there is no remaining relic and so there is no residual noise to remove.

2. EXPERIMENTAL

Enclosing the experiment are two large concentric vacuum flasks referred to as “dewars” that contain liquid cryogenics. They were produced by Pope Scientific out of borosilicate glass and silvered on the inside to reduce radiative heating and minimize vaporization of the cryogenic fluids. Optical access is provided by ~2cm slit along the axes of the dewars that were unsilvered. The outer dewar, or “nitrogen dewar”, was used to insulate liquid nitrogen from the laboratory and so the cavity inside was pumped down to 10^{-7} Torr and baked. The inner dewar, referred to as “helium dewar”, was also pumped to this level but then backfilled with 1 Torr of nitrogen to couple the inner dewar to the outer dewar at higher temperatures thus reducing the time for thermal equilibrium to be reached. Once liquid helium was contained in this dewar, the nitrogen molecules were adsorbed on its walls and therefore did not cause any heat leaks.

The helium dewar fill volume could hold approximately 6 liters of helium. This allowed for approximately 4 hours of experimental operation. Operating at low temperatures inside the dewar required the helium vapor to be pumped away using an Edwards EH 1200 Roots blower and an Edwards E2M80 two stage mechanical pump. The combination of pumping produced pumping speeds for helium vapor of 233 liters/second. This is necessary in order to maintain temperatures below 1.4K although optimal conditions could have

provided temperatures as low as 1K. The temperature is measured by a Lakeshore germanium thermometer calibrated for the temperature range of 0.3 K to 20 K. Control of the temperature in the dewar was obtained simply by throttling the external pumping rate.

2.1 Fountain effect

In earlier studies using this apparatus [31], impurity helium condensates were prepared in a small beaker inside the dewar that was filled with superfluid helium with a fountain pump. The superfluid helium is drawn up to the beaker by the fountain effect. The property of helium that is referred to as superfluidity is that it flows with zero viscosity and will flow through highly restrictive geometries as if there is no boundary or constriction even at near atomic scales. Superfluid helium will creep along a hydrostatic gradient created by thermal or pressure gradients [32]. The flow of superfluid helium is best described by the two fluid model where the helium can be thought of as consisting of two interpenetrating components, the superfluid component and the normal component. Only the normal component can interact with the walls whereas the superfluid component exhibits frictionless flow [33]. In this experiment a thermal gradient is provided by applying heat from a small resistive heater to a stainless steel cylinder containing a fine powder which provides what is referred to as the superleak or the pathway for superfluid helium to flow and leave behind the so called normal helium. The superfluid component will flow rapidly toward a heat source and will exhibit frictionless flow through the fine powder eventually reaching the sample

collection beaker as described by Landau and Tisza in their two fluid model of superfluidity [34]. The resulting fountain pressure pushes the superfluid helium up a thin stainless steel capillary that leads to a collection beaker. During sample preparation the stainless steel cylinder is heated which thermally decouples the heater from the helium bath. When current is supplied to the resistor it dissipates heat into the helium in the fine powder causing a thermal gradient that is equivalent to gouging a hole into the bottom of a tank of fluid [35]. If the flow is stationary and of small velocity, the mechanical flow follows a linear equation derived by London and is often referred to as the London equation [36].

$$\nabla p = \rho s \nabla T \qquad [4]$$

Where *p* is the pressure, ρ is the density, s is the entropy, and of course T is temperature. This describes the thermo-mechanical effect of superfluid helium, that is when heat is supplied, the superfluid component of helium flows towards the heat source. However, the normal component follows the typical Poiseuille flow of standard fluid dynamics which is typical for ordinary liquids [37]. For this experiment the superfluid helium is guided into the capillary and up to fill the beaker and the normal fluid is left in the bath. The sample beaker will be continuously filled with superfluid helium as long as current is supplied to the heater and there is enough superfluid helium to sustain stationary flow up the capillary [38].

2.2 Optical systems

The spectrometers used in the experiment include two systems, one from Andor Technology and another from Ocean Optics. The system from Ocean Optics is a closed system with onboard memory, HR4000 model, capable of being responsive from 200nm to 1100nm, and shutter speed of 10 microseconds to 4 milliseconds. This was used to keep a backup record of all experiments and as an in situ monitor of integrity of the high resolution spectra using the Andor system. Both systems were connected via a “tee” to an optical fiber leading from the slit in the dewars so they could simultaneously take spectra from the same source.

The Andor system included a spectrometer, model Shamrock 500i, that is based on a Czerny-Turner grating design with three gratings that could be exchanged with a wavelength reproducibility of $\pm$0.05nm. The spectrometer was coupled to an external camera that was also from Andor Technology, model Newton EMCCD. This system had superior timing and resolution due to thermoelectric cooling of the CCD inside the camera that the Ocean system lacked and faster register speed. In future work the spectrometer will be equipped with an Andor camera model iStar, which has significantly faster registration speed.

2.3 Cold jet preparation

Preparation of impurity helium condensate samples was based on a technique pioneered by Gordon, et. al. [39] The process consists of producing a

narrow and well directed jet inside a helium cryostat with formation of a solid made up of nanoclusters containing impurity atoms or molecules ordered like a molecular solid in superfluid helium that is near 1.5 K [40]. Concentrations of stabilized free radicals form in the nanoclusters because of rapid heat transfer from superfluid helium and high specific heat of liquid helium. Diagrams of the experiment are in figure (2.1). In this work our samples were prepared using an identical method but only trace amounts of oxygen or other impurities were contained in our helium mixtures. Concentrations of the impurities were so small that solid nanoclusters were not formed in our sample collection beaker. While data was being taken for the impurity helium samples it was noticed that there was an unidentified peak at 543nm and 777nm. Later this was determined to be from the oxygen emission lines.

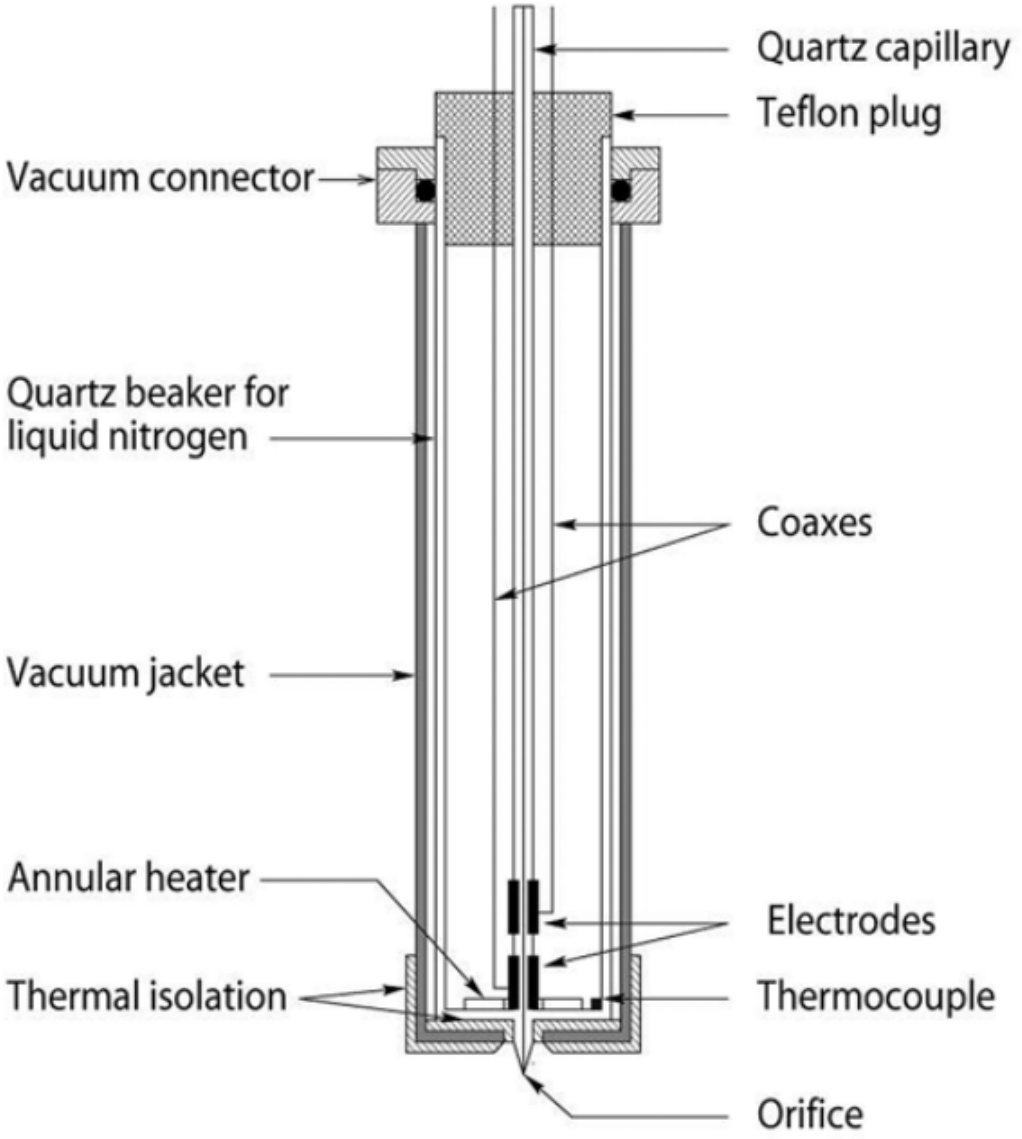

FIGURE

Figure 2.1: Diagram of the discharge and orifice origin. Jet of atoms and molecules inside the cryostat flow through the capillary and are excited by the electrodes before flowing through the orifice creating a jet [40]. Prepared admixtures flow down through the quartz capillary and into a region between the electrodes that excite the gas from outside the capillary and then the atomized gas flows out of the orifice. Reprinted with permission from [40].

The setup is meant to produce a supply of atoms and molecules through a gas handling system that prepares and stores mixtures of 1/20 up to 1/1000. The gases used are from Linde Electronics & Specialty Gases and have a purity of 99.9999 or 6.0 purity. As mentioned earlier there is also a vacuum pump system for pumping helium vapor from the cryostat to keep the environment cooled. The quartz capillary is cooled with liquid nitrogen contained in an outer quartz tube. The capillary tip is 0.75mm in diameter through which one can create a Gaussian jet emerging from the tip. Ring electrodes outside the capillary provide a radiofrequency electric field, concentric with capillary, made out of copper. The electrodes are connected to an RF matching network, which was in turn connected to an HP8656 frequency synthesizer. The signal was amplified by an ENI3100L that amplifies the signal from the frequency synthesizer by about 50dB. Finally a laboratory built inductor-capacitor was provided to frequency match the electrodes to ~52MHz. The lower electrode is placed near the orifice in order to provide some heat to prevent any freezing that may plug the orifice. Species formed in the discharge then “emerge” from the orifice into the pumped helium cryostat. This process creates a “plasma needle” similar to those used in medical applications of plasmas.

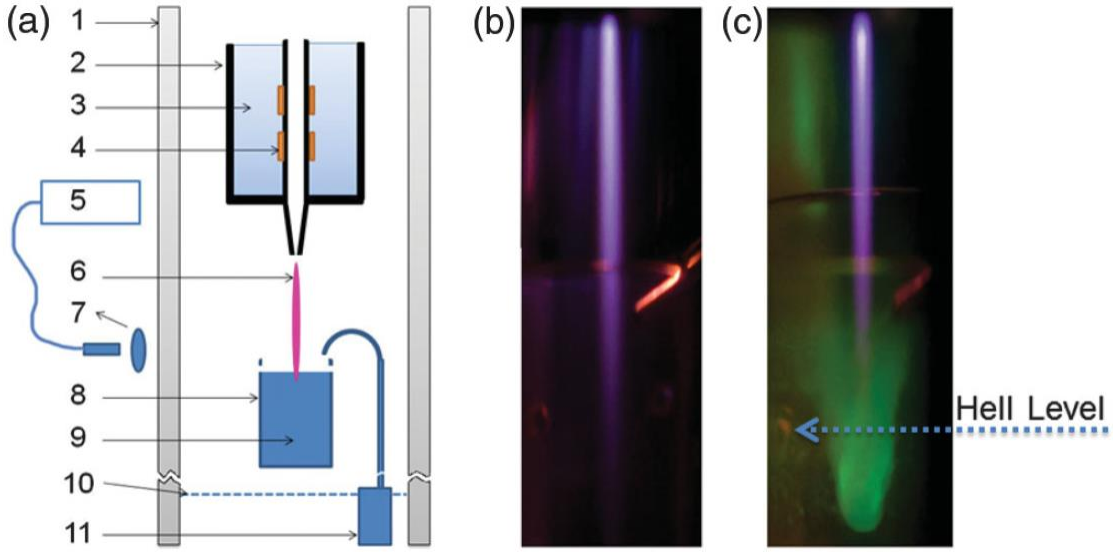

FIGURE
Figure 2.2: (a) Diagram of the jet and beaker setup. 1: helium dewar, 2: quartz tube, 3:liquid nitrogen, 4: RF electrodes to excite the gas flowing through the capillary, 5: optical spectra collected via fiber optic, 6: jet of excited neutral atoms, 7: large aperture lens, 8: quartz beaker with liquid helium surface, 9: superfluid helium inside the beaker, 10: level of liquid helium in the bath below the beaker, 11: fountain pump supplying the beaker. (b) picture of the jet without liquid helium in the beaker, fountain pump tip is reflecting light coming from the discharge region. (c) picture of the jet inpinging the surface of liquid helium indicated by the arrow. The turbulence of the jet creates a crater of about twice the diameter of the jet and approximately 0.3 cm deep in the liquid helium that glows green with the oxygen emission lines. Reprinted with permission from [59].

Sample gas admixtures are fed from the gas handling system to a flow controller from Brooks Instruments (5850E) which feeds into the capillary that is aimed at the collection beaker ~2cm below the orifice. The fountain pump constantly provides superfluid helium to the beaker to keep it full and to compensate for vapor losses. The jet produced is illuminated by luminescence from highly excited states in the species contained in the mixture. For a typical oxygen impurity content of several ppm in the helium tank the flow is 3×10^{14} atoms per second. Control of impurities in the sample is done by adding more through the gas handling system or reducing the concentration by using a cold trap prior to introducing the gas to the system due to the higher condensation temperature of oxygen.

Power deposition from the capacitively coupled RF discharge raises helium to its metastable states via electron impact and the metastables travel down the jet that impinge onto the liquid helium surface. The metastable He atoms and molecules (He^* and He_2^*) transfer their energy along the jet and at or near the surface produce strong luminescence. The light travels in all directions and through many surfaces that are not of optical quality so that much of the information about emission rates and source positions in the jet is not clear. Light is collected via a lens coupled optical fiber with a large numerical aperture and positioned via a controller to allow for vertical movement. Origins of light collected from the surface or reflections off of the dewar surfaces could not be discerned from light from the jet or the fairly deep crater produced by the

impacting jet. However, a measurement of vertical position and light collection did produce significant differences in light intensity in the spectra and using molecular nitrogen in the jet, the rotational spectra provided temperature determinations versus vertical position which changed as expected, with higher temperatures being near the capillary orifice and lower temperatures at the liquid helium surface. The limitations of this method for accurate temperature determinations at the lowest temperatures are discussed later.

Impurity-Helium mixtures move coaxially with the jet that thermalizes via collisions and the relative velocity of impurity to helium atoms becomes negligible along the jet, allowing the study of processes that take longer than single collisions in the gas phase. In addition to cooling the surface of the liquid, helium plays a substantial role in what processes of emission dominate the spectra. In particular metastable transfer is enhanced by the trapping of impurities in the crater formed by the jet in the liquid helium.

2.4 Emission studies

Spectra of the emission in the jet were studied while sample beaker was empty, during filling, and while it was maintained by the fountain pump as shown in figure (2.3). The pressure inside the helium dewar was varied to study the dependence on density by adjusting the pump speed. To further study the density dependence of oxygen it was either added to mixture in trace amounts or removed via a cold gas trap.

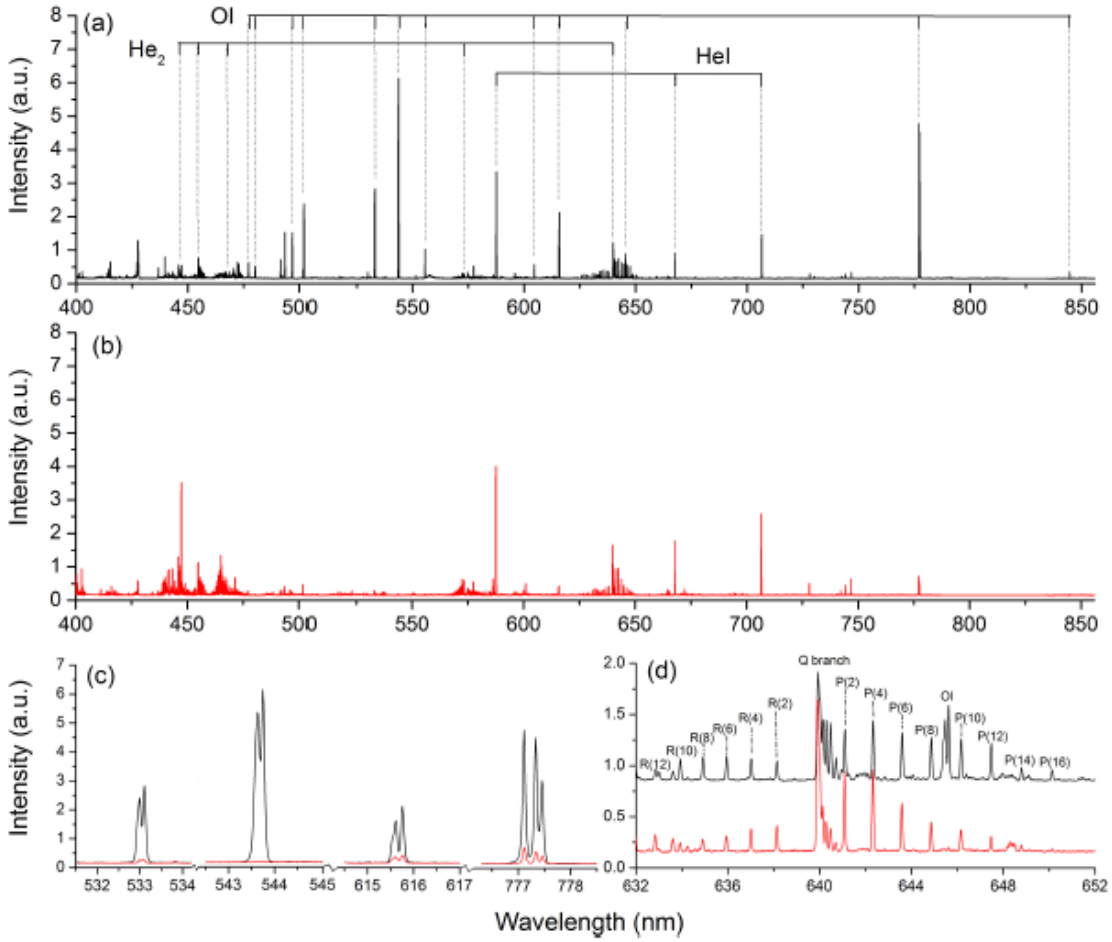

FIGURE

Figure 2.3: Spectra taken with trace oxygen (1ppm) in helium jet. (a) with the beaker full of superfluid helium, (b) with the beaker empty, (c) high resolution of the atomic oxygen lines with higher intensity lines being with the full beaker, and (d) high resolution of molecular helium lines with above spectra being the full beaker and lower empty beaker shifted to show contrast. Reprinted with permission from [41].

Also an interesting phenomenon was when the liquid helium was filling the beaker. This is shown in figure (2.4) and the interesting part is the molecular helium (curve 3) response while the beaker is filling. The helium atomic lines decrease in intensity and the molecular helium lines and atomic oxygen lines increase but there is a maximum where molecular helium then decreases. This suggests the process that creates molecular helium competes with the excited oxygen. The hypothesis that the molecular helium contributes to exciting oxygen through metastable transfer is supported by this.

There is some structure to the spectra as the beaker is being filled. The oxygen multiplet response shows the same structure as the molecular helium. Atomic helium on the other hand doesn't have much structure other than an exponential tail to a lower intensity and then flattens out.

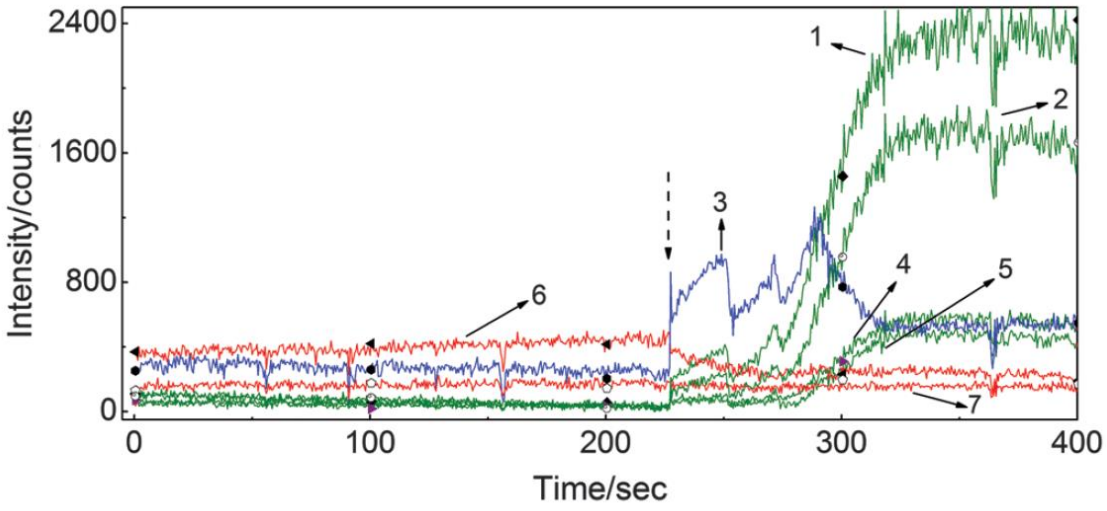

FIGURE
Figure 2.4: Time dependence of the spectra due to the filling of the liquid helium beaker. Atomic oxygen lines 1: 543 nm, 2: 777 nm, 4: 616 nm, and 5: 533 nm. Curve 3 is the measured molecular Helium lines 640 nm. Atomic helium lines 6: 588 nm and 7: 707 nm. The dotted arrow indicates the moment that liquid helium begins to fill the beaker. Reprinted with permission from [59].

Figure (2.5) shows the effect of a full beaker versus an empty beaker. The atomic oxygen lines that lead to the 777nm multiplet in the high resolution spectra are measured by the Andor spectrometer and are markedly reduced while the helium atomic lines are increased. The presence of the liquid helium barrier therefore encourages molecular helium production and up closer to the jet plume will produce much higher quantities of highly excited oxygen through metastable transfer. The empty beaker produces higher intensity in the lowest wavelength of the 777 nm multiplet. This is not the case for the full beaker, which has the middle wavelength of the 777 nm multiplet as the maximum of the multiplet. This means that the empty beaker behaves more like a lifetime limited transition probability for the 777 nm multiplets and the full beaker does not follow the lifetime limited transition probabilities and there is a process providing a definite difference as indicated by intensities inside brackets of figure (2.7). The full beaker increases the effect of the metastable transfer as compared with the empty beaker as would be expected for lower temperatures and higher collision rates.

By increasing the density of the oxygen by adding it to the helium source gas, it was observed that the oxygen atomic lines increased and the molecular helium lines disappeared. The oxygen trace gas population was reduced through pumping the helium source gas through a cold trap before entering the discharge region. This reduction resulted in the oxygen lines decreased and the helium lines increased.

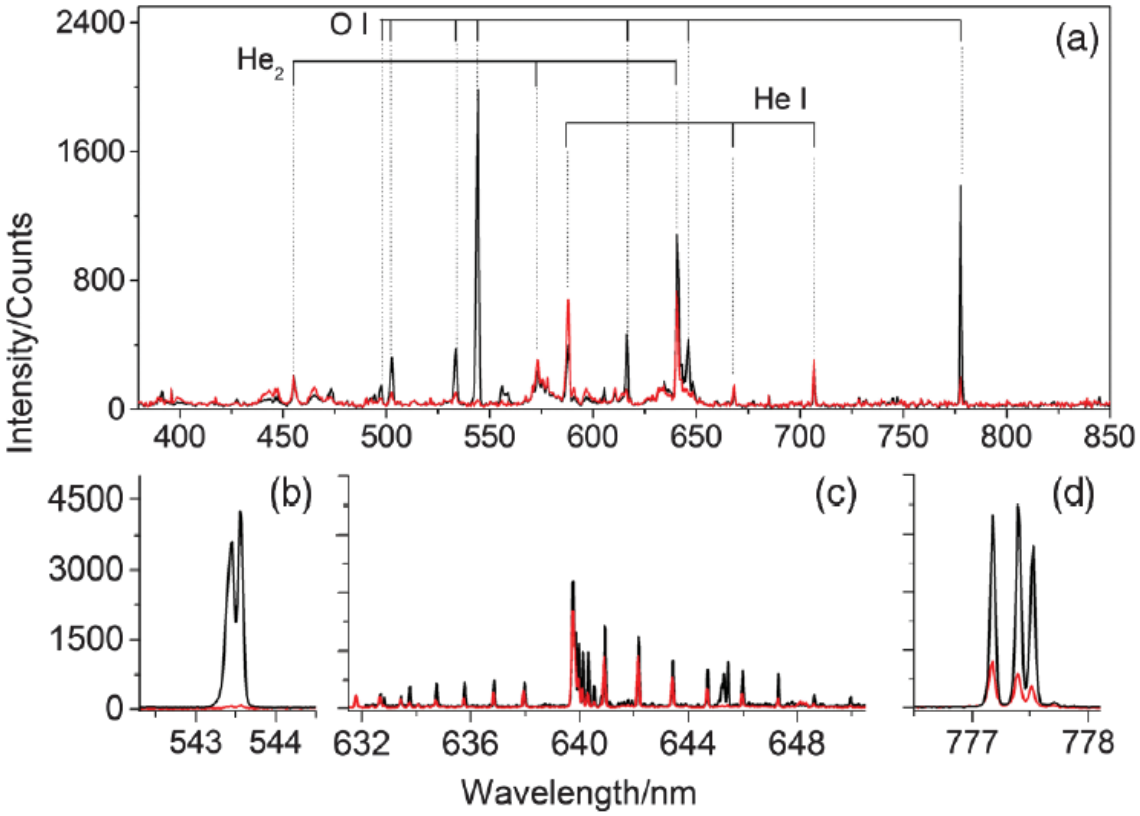

FIGURE

Figure 2.5: Dependence of helium jet on density of oxygen, (a) when the beaker is empty corresponds to lower intensity curve and higher intensity curve is when the beaker is full. (b) high resolution of atomic oxygen line at 543 nm shows splitting but not three peaks; largest intensity is the largest wavelength as follows from lifetime transition probabilities. (c) Molecular helium high resolution at 640 nm showing almost no change. (d) high resolution of atomic oxygen 777 nm lines showing clearly three peaks for the multiplet with the middle wavelength showing highest intensity for full beaker and the lowest wavelength showing highest intensity with beaker empty. Reprinted with permission from [59].

TABLE

Table 2.1: Identification of observed spectral lines from atomic oxygen and both atomic and molecular helium in this work. Reprinted with permission from [41]

λ, nm	Transition	λ, nm	Transition
844.6	O I ($3s^3S$-$3p^3P$)	728.3	He I ($2p^1P$-$3s^1S$)
777.4	O I ($3s^5S$-$3p^5P$)	706.5	He I ($2p^3P$-$3s^3S$)
645.4	O I ($3p^5P$-$5s^5S$)	667.9	He I ($2p^1P$-$3d^1D$)
615.7	O I ($3p^5P$-$4d^5D$)	587.6	He I ($2p^3P$-$3d^3D$)
543.6	O I ($3p^5P$-$6s^5S$)	501.6	He I ($2s^1S$-$3p^1P$)
533.0	O I ($3p^5P$-$5d^5D$)	639.6	$He_2(d^3\Sigma_u^+ \rightarrow b^3\Pi_g)$
502.0	O I ($3p^5P$-$7s^5S$)	573.2	$He_2(f^3\Delta_u \rightarrow b^3\Pi_g)$
496.8	O I ($3p^5P$-$6d^5D$)	454.7	$He_2(h^3\Sigma_u^+ \rightarrow b^3\Pi_g)$

Earlier work by Popov and colleagues [42] shows the oxygen lines of interest, specifically the 543nm line, but identification of it was not made and left as an unknown. It was only after using the high resolution spectrometer that a complete identification could be made available. When the beaker is empty, a rich spectra of neutral molecular and atomic helium lines dominate the spectrum with three neutral atomic oxygen lines present. As the sample beaker is filled with liquid helium, atomic oxygen lines tend to dominate the spectrum and reduce the molecular helium lines to almost zero intensity. Environmental factors that increased oxygen atomic line dominance in the spectra were investigated. Pressure plays a key role in reducing all of the peak heights due to pressure broadening and enhanced non-radiative processes that de-excite the atoms. The atomic oxygen lines were most pronounced in the range of 20-200ppm of O_2 content in the jet of helium. Atomic helium lines were practically not affected by the change in O_2 content in the jet. Molecular He-He bands decrease with respect to the other lines in the spectra with the added O_2 content in the mixture. It is suspected that this phenomena is due to energy transfer to oxygen atoms which is made more readily available with more oxygen added.

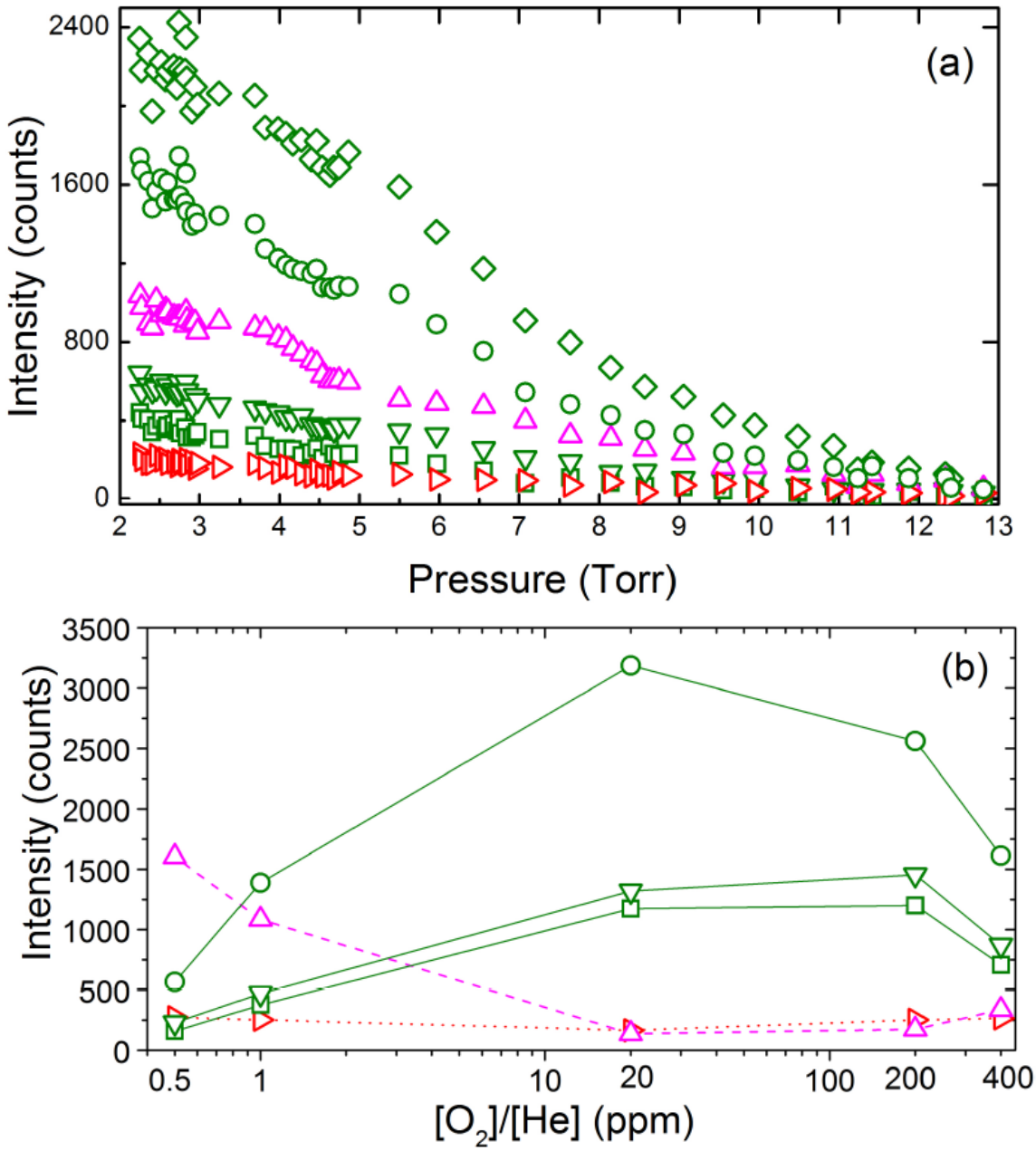

FIGURE

Figure 2.6: Pressure and admixture density ratio dependence of emission (a) dependence of the atomic oxygen and both atomic and molecular helium lines on the pressure inside the dewar. (b) dependence of lines on ratio of oxygen to helium densities of the sample gas added to the system. ◊ O-line (543 nm), ○ O-line (777 nm), Δ Helium molecular band (640 nm), ∇ O-line (615 nm), □ O-line (533 nm), ▷ Helium atomic line (707 nm). Reprinted with permission from [41].

The average travel time of from exit of capillary to the superfluid helium surface is of the order of 10^{-4} seconds, so that states with spontaneous emission rates of 14-1000 ns should de-excite at the exit of the capillary. Observed emission from these states in the jet must be due to processes inside the jet itself. The impurity species are so rarefied that they are unlikely to recombine with their pair atoms forming O_2 or N_2 and so the energy transfer required to excite them to higher states after emission can be obtained mainly from metastable states of atomic and molecular helium through collision processes in the jet. When nitrogen is introduced into the jet intentionally with density comparable to helium it forms N_2 and rich molecular nitrogen lines dominate the spectrum. The temperature of oxygen determined using intensity ratios for the atomic oxygen lines is orders of magnitude higher than when liquid helium is in the beaker, as might be expected since the temperature in the latter case is much lower. The number of collisions expected for the gas density is several times more than needed to reach thermal equilibrium with the helium vapor according to the Doyle calculation [43] which will be discussed later. The difference in the light collected in the presence of liquid helium and the absence of liquid helium must therefore be from processes occurring at and just above the surface of the liquid helium.

2.5 Jet interaction with liquid helium surface

A molecule can do one of two things when encountering a surface, it can either be stuck to the surface or it can be reflected back into the gas phase by

the surface. When a molecule is stuck to a surface it can remain on the surface for some time and then return to the gas phase, characterized by what is called the coefficient of accommodation, or it can stay stuck to the surface and eventually be adsorbed into the bulk material. One way these stuck molecules can influence the behavior of later impinging molecules is that they will impede the way between another molecule and the bare surface. To improve the odds of being reflected back into the gas phase, more molecules should reside on the surface. Most of these molecule-molecule collisions on the surface can be assumed to result in reflection from the surface and will not contribute to further adsorption to the bulk material. Langmuir used this as his starting point when developing his description of adsorption which leads to a theoretical limit of adsorption [44]. The adsorption limit will be when the surface is covered with an adsorbed layer of closely packed molecules and no further adsorption can take place and all new molecules will be reflected off the surface much like the way in which light or billiard balls are reflected off surfaces. Langmuir's description does help to explain the formation of the crater formed around the jet and liquid helium surface. The average depth of the crater was about half a centimeter which does not correspond to the equilibrium between the energy flux of the jet and the surface tension of liquid helium, which is about 0.4 erg/cm^2, and so one is left to conclude there must be some lingering molecules and atoms on the surface aiding the reflection of energetic molecules hitting the surface from the jet. The absence of molecular oxygen spectral lines in our measurements

supports this description because the density of oxygen is so low that the probability of two oxygen atoms to find one another and recombine is very low compared to a helium atom colliding with an oxygen atom. The oxygen lingers in the crater and rebounds off the surfaces of the crater that has a protective layer of atoms from the jet that are stuck to the surface. Thus the chance that an oxygen atom obtains energy from a metastable helium atom flowing down the jet is enhanced and the temperature of oxygen is such that the measured intensity of the upper states providing the 543nm and 533nm green lines increases because many of the atoms are cycled through the ground and higher states through more frequent collisions with metastable helium atoms or molecules travelling down the jet. These higher states of oxygen are rarely seen unless it is in a recombination scheme with ions and electrons. The metastable states just below these that generate the green and two red lines, 558nm or ^{1}S, 630nm, and 636nm from the ^{1}D state that are typically seen in aurorae and in the comae of comets [45] are well known and de-excite through the 777nm multiplet as seen in this work; however this work is unique because the other two branches that go through the 777nm multiplet are virtually absent.

2.6 Helium-neon comparison

The metastable transfer of energy from helium to oxygen is analogous to the transfer of energy between helium metastables and neon [46]. Measurements for the reaction rates of neon and helium are well studied [47] whereas the reaction rates for oxygen and helium are less well studied,

especially at low temperatures. Inside an active discharge helium in the 2^1S state is quickly converted to 2^3S state by electron collisions. The helium 2^3S state is nearly resonant with the neon lowest level excited states of configuration $2p^5 3s$ which has four levels, two of which (^3P_o and $^3P_2$) are metastable while the other two are short lived by resonance. Collisions with ground state neon atoms and helium metastable 2^3S will produce excited state neon in the process of collision.

$$\mathrm{He}^*(2^3S) + \mathrm{Ne} \rightarrow \mathrm{Ne}(2p^5 4s \text{ and } 2p^5 3d) + \mathrm{He} \quad [5]$$

This process is what was observed and confirmed by Javan and colleagues [17] while studying the helium neon gas laser mechanisms. The reaction rate (k_1) has been measured several times, first by Phelps [48] which yielded a value of $2 \times 10^{-12}\mathrm{cm}^3\mathrm{sec}^{-1}$ and second by Javan's group [17] at a pressure of a few Torr that yielded a value of $5 \times 10^{-12}\mathrm{cm}^3\mathrm{sec}^{-1}$ using a stationary afterglow system. Flowing systems have improved the accuracy of the coefficient since then.

Could this be extended to molecular helium? It has a metastable state that could very well do the same kind of transfer. Published measurements of the reaction of the metastable helium molecule and neon is hard to find, and with oxygen even more scarce. Looking at the reaction that dissociates the helium and excites the neon one can plausibly guess that this is a likely reaction.

$$\mathrm{He}_2^*(a^3\Sigma_u^+) + \mathrm{Ne} \rightarrow \mathrm{Ne}^* + 2\mathrm{He} \quad [6]$$

Direct measurements of this reaction rate were made by Phelps [48] with a surprising value of $3\times 10^{-11}\mathrm{cm}^3\mathrm{sec}^{-1}$ that is roughly the same order of magnitude as the atomic reaction; other investigators found values from $4.4 \times 10^{-11}\mathrm{cm}^3\mathrm{sec}^{-1}$ [47] to $2.1 \times 10^{-10}\mathrm{cm}^3\mathrm{sec}^{-1}$ [49].

2.7 Non-radiative transfer

The mechanism of the energy transfer is referred to as transferring energy non-radiatively which occurs if the emission probability of the metastable atom overlaps the absorption of the neutral atom in frequency or in wavelength and there are mechanisms that would broaden these curves discussed later. If the energy difference of the maximum of the absorption and the emission is small compared to the energy of the emission, then non-radiative transitions can occur. Short range mechanisms start to develop when this energy difference in frequency is comparable to the rate of collisions, and when the rate of collisions is much less, then it almost becomes exclusively through dipole-dipole interactions that the transfer is possible. This understanding must have been known by those involved in the discovery of the helium and neon laser. The active medium inside the cavity has a size that directly influences the radiative emission efficiency but it does not change the non-radiative efficiency although it is important to note that both depend on the spectral overlap. The overlap

between metastable helium atoms and molecules and the high-lying states of neutral oxygen must be small even for fast moving collisions because the ionization energy for neutral oxygen is ~14eV. There is a possibility that the polarizability of the metastable helium could allow for a strong Stark shift of the energy level that would allow for more overlap of the oxygen energy level. The process of using a Stark shift to induce a nonradiative resonance is called "Förster resonance." [50] However, it is not expected for there to be anything other than the local field involved in the collision process so the shift would be small unless one or both collision partners had a built in dipole moment [51].

Mixtures with helium and nitrogen are often used to determine purity of helium mixtures but in many cases oxygen had been present almost always without detection. P. Emmott and R. E. Wilson observed that oxygen introduced into a helium-nitrogen admixture at low densities tended not to interfere with the internal standard of measuring nitrogen to helium density ratios using luminescence. The ratio of emission for nitrogen versus helium, $(I_{358}/I_{502})^2$, or the square of the ratio of intensities of nitrogen line at 358nm and helium line at 502nm plotted against the nitrogen content gives a straight fit line for which one can determine the density of nitrogen in a helium-nitrogen admixture [52]. In such a mixture the effect of oxygen content left the ratio unaffected up to 0.04% even though it was seen by the observes to change the line intensities but the ratio was unchanged. Therefore the interaction with helium and oxygen does not interfere with the individual reactions between nitrogen and helium. This is

one of the reasons why the oxygen and metastable helium transfer effect being described in this paper is useful because oxygen also does the same type of interaction that helium and neon do in the helium and neon laser but does not interfere with the nitrogen-helium interactions.

The metastable helium state is ~20eV, which is a few eV higher than the ionization potential of the oxygen atom. Observations of the spectra from metastable transfer from helium to oxygen would then be expected to exhibit ionized oxygen lines but in this experiment they are absent entirely which follows from the assumption that all the constituents of the mixtures are sufficiently recombined and of neutral charge after leaving the discharge region of the jet. Metastable helium finds an oxygen atom and forms a quasi-molecule during the time it would take for the excited electron in helium to make one orbit around the helium atom. After becoming unstable and dissociating, the oxygen and helium atoms carry away the excess energy which for the helium atom must be purely translational and the oxygen atom is left in a high energy internal state but not ionized.

For low temperatures, the rate of radiative transitions of the metastable helium atomic state drop significantly. For temperatures above 100K the rate coefficient for radiative transitions from metastable helium was calculated by Zygelman [53] which corresponded to the measured rate coefficient at room temperature by Payne and colleagues [54] to be on the order of $10^{-14}\mathrm{cm}^3\mathrm{s}^{-1}$. The rate below 100K appears to follow a decreasing trend to less than

$10^{-16}\mathrm{cm}^3 s^{-1}$, which would be expected for long travel times of metastable helium in a jet that contains few collisions. Further research into collisions of helium with atom-atom and atom-molecule interactions found that at temperatures below 4.2K the rate of collisions are suppressed and in experiments using electron avalanches the contribution of highly excited helium inducing ionization is negligible [55]. The effect of highly excited helium inducing ionization is a well-known process that pollutes the study of electron avalanches so much that it is named [56] the "Holbeck-Molnar process." For gases of temperatures higher than liquid helium the effect must be corrected for but at temperatures below liquid helium the effect is vanishingly small. This implies that metastable helium is less likely to ionize atoms or molecules through collisional processes at low temperatures.

For the process of transfer of energy from one atom to another, i.e. $A^* + B \rightarrow A + B^*$ also known as "collisions of the second kind," initial and final states are more likely to overlap. This can be understood as a potential curve crossing. If both collision partners approach each other on one potential curve that crosses another potential curve that leads to the other partner in an excited state and when they separate again they can do so on the other potential curve. Inspection of potential curves involving one excited and one ground state atom would yield a crossing point much higher than the excitation energy of the A and B atom, which means in traditional "closest approach" models, the relative kinetic energy of the collision partners, $\frac{1}{2}\mu v_{rel}^2$, would have to be larger than the

energy of excitation of both. In the case of metastable helium and oxygen the relative velocity would have to be on the order of $>10^5$ m/s and that seems quite unrealistic. However, oxygen does have high-lying states that are spin allowed but they lie above the ionization continuum. These states are referred to as "auto-ionization states" because they typically de-excite by ejecting an electron and the final state is $O^+(^4S)$. Since these states have a finite lifetime [57] this would mean the excited atoms could conceivably de-excite radiatively through a third body process instead of auto-ionizing and thus creating the high-lying states of oxygen seen in the experimental spectra. The total cross section of photon absorption of atomic oxygen has a noticeable increase of nearly an order of magnitude at precisely 20.53eV with a width of about 2.2eV which lies squarely at the ~20eV of the metastable helium states [58]. Thus by the requirement of non-radiative transitions, both emitting and absorbing states clearly overlap. These states could be the means for energy transfer from metastable helium to oxygen without ionizing the oxygen atom because the time it takes to self-ionize is long compared to the collision time of oxygen to another helium atom. The collision time in this experiment is expected to be around 3ns near the surface of the liquid He II [59] comparable to the measured atomic oxygen auto-ionization states, ~0.8ns, that lie in the energies around 20eV [57]. According to selection rules the de-excitation from these auto-ionizing states would force the oxygen atom to follow the de-excitation scheme that follows the

777nm multiplet that produces the lines seen in this work and does not produce the lines that are absent.

The temperature of the gases in the jet before entering the bulk superfluid helium should be near the same temperature as superfluid helium. During slow atomic collisions, meaning the relative motion of the two nuclei involved is slower than the orbital velocity of active electrons, the interaction can be viewed as a formation of a quasimolecule. Since the species in the jet are moving collinearly one can expect the formation of quasimolecules at the termination of the jet inside superfluid helium. Near the surface this effect is enhanced in analogy with the effect in merged cold molecular beams [60].

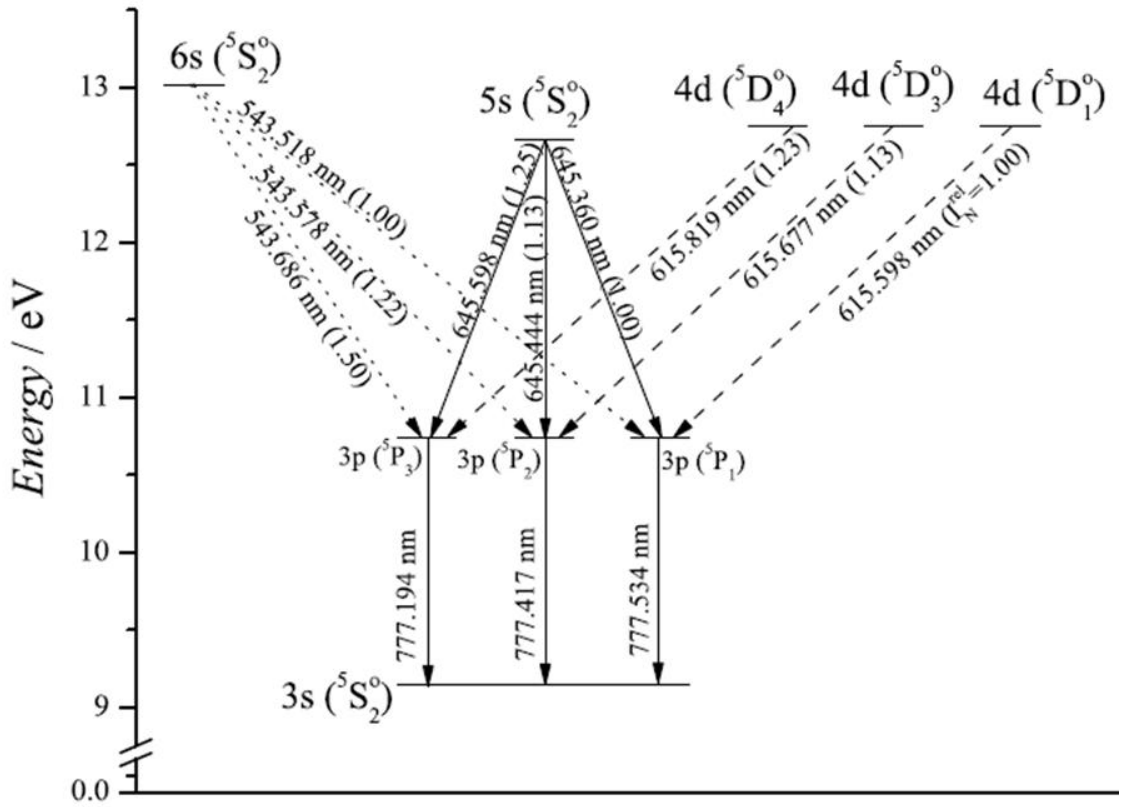

FIGURE

Figure 2.7: Energy level scheme of 777nm emission multiplet of atomic oxygen. The values in parentheses are the normalized intensity within this multiplet (normalized to the $^5D^0_1$ line) using the transition probabilities calculated by lifetime of the states. In this work the 543nm lines are measured as more prominent than by a factor of two than the others, suggesting a preference to decaying through that channel other than lifetime considerations. Reprinted with permission from [61].

2.8 Atomic oxygen multiplet

If an excited state has multiple radiative paths to de-excite then the total transition rate can be written as the inverse of the sum of the inverse of transition lifetimes from initial to final states. In terms of the energy levels of oxygen as previously discussed the 543nm emission has a single initial state and three final states.

$$\tau_i{}^{-1} = \sum_f \tau_{i\to f}{}^{-1} \quad [7]$$

N systems in the initial state will transition to the final state by

$$N(t) = N_0 exp\left(-\tau_i^{(s)} t\right), \quad [8]$$

in which the mean transition rate for the i-th state can be written as:

$$\tau_{mean} = \frac{1}{\tau_i} \quad [9]$$

So for the case of the ${}^5S \rightarrow {}^5P$ transition of atomic Oxygen the expected transition probability should be 3.86 x 10^5 s^{-1}, given that the triplet states have transition probabilities of 0.774, 1.29, and 1.80 x 10^6 s^{-1} for the J=1, 2, 3 states respectively [61]. The following de-excitation pathways have a much larger transition rate (~35 x 10^6 s^{-1}) such that there could be a population inversion between those states in which lasing could occur and the 777nm multiplet, see

figure (2.7). The observed luminescence also gives rise to thoughts about creating a lasing medium inside a crater of liquid helium. Control of the flow rates could minimize the turbulence of the crater and therefore losses in the surfaces that would contribute to losses in a coupling regime to an optical cavity.

2.9 Buffer gas cooling

Nonflammable and inert gases make good buffer gases that add pressure to a system to limit and control the speed of combustion of an oxygen admixture. Another use of buffer gases is to reduce contaminants in-between seals in compressors and vacuum pumps. More recently their common uses include adding collisions to admixtures in order to reduce or enhance photochemical processes.

Buffer gas cooling is the method of dissipating translational energy through collisions with slow moving buffer gas atoms or molecules in order to thermalize to low temperatures. It is similar to evaporative cooling of a closed ensemble in that it utilizes elastic collisions. The method doesn't rely on internal energy structure or electric dipoles so that any target species can be used as long as it can survive multiple collisions with lower energy companions. Most common species have little or no vapor pressure at low temperatures except for He and so He is the ideal choice to reduce temperatures to below a few Kelvin.

The cooling process can be modeled by assuming totally elastic collisions between two mass points. Using a low density of molecules compared to helium one can assume that only molecule-helium collisions occur. Assuming hard

spheres and ideal gases, one can calculate the temperature of oxygen atoms due to collisions with the cold helium vapor. Following a calculation attributed to John Doyle's group at Harvard [62], after thermal averaging one can write the temperature difference between the buffer gas, T_B, and the temperature of the oxygen atoms, T_O, by a relation due to the mass difference. [43]

$$\Delta T_O = -\left(T_O - T_B\right)/\kappa, \quad \kappa \equiv \frac{(m_B - m_O)^2}{2m_B m_O} \qquad [10]$$

The temperature of the oxygen impurity after *N* collisions changes as a function of the temperature of the buffer gas, as given by:

$$T_O(N) - T_O(N-1) = -(T_O(N-1) - T_B)/\kappa \qquad [11]$$

If *N* is large and the change of temperature due to one collision is small one can write the difference as a simple first order differential equation.

$$\frac{dT_O(N)}{dN} = -(T_O(N) - T_B)/\kappa \qquad [12]$$

Solving the equation yields for the ratio of temperatures a simple exponential expression. In the interest of completeness the steps of the calculation are written out explicitly here. First step is to multiply to get temperature on one side of the equation.

$$\frac{dT_O(N)}{-(T_O(N)-T_B)} = dN/\kappa \qquad [13]$$

Integrate both sides and put in limits for both sides for zero collisions to *N* collisions.

$$-ln(T_O(0)-T_B) + ln(T_O(N)-T_B) = ln\left(\frac{T_O(N)-T_B}{T_O(0)-T_B}\right) = -N/\kappa \qquad [14]$$

Exponentiation and multiplying both sides by $T_O(0)-T_B$ gives

$$\frac{T_O(N)}{T_B} = 1 + \left(\frac{T_O(0)}{T_B} - 1\right) exp(-N/k) \qquad [15]$$

For large temperature differences, in other words $T_O(0) \gg T_B$, or more explicitly the ratio of temperatures prior to any collision is large compared to one, so the equation can be written in a more familiar way.

$$\frac{T_O(N)}{T_B} \approx 1 + \frac{T_O(0)}{T_B} exp(-N/k) \qquad [16]$$

This expression allows for a solution of the number of collisions required to reduce the temperature of the oxygen atoms or other impurities to a certain temperature by knowing what the temperature of the buffer gas or the helium vapor is in the experimental setup. This in turn can be used to calculate the time required to reach equilibrium by using the density of the buffer gas to calculate

the time required for one collision and multiply by the number of collisions. For the temperatures used in the experiment discussed here less than 100 collisions should be enough to reduce the temperature of the oxygen atoms to the temperature of the helium vapor.

However, there are some deviations from this if the target molecule has internal degrees of freedom, such as the case of molecules with rotational and vibrational degrees of freedom. Metastable collisions with a partner that have high rotational excitation level probabilities leave a channel for energy to be taken away from the system in the form of a “hot” molecule, i.e. one that will transition to lower states as if it had been in a hotter temperature distribution. This would result in a non-linear Boltzmann distribution. Particularly this is the case with nitrogen molecules and so a temperature determination using nitrogen requires knowledge of the higher level or hotter molecule density. Another issue that can occur is that the molecule taking away energy in the form of internal energy will have long-lived states as compared to the time it takes for the molecule to traverse the vessel containing it which would also be represented as a hotter molecule distribution. Modelling the behavior as separately interacting systems provides the ability to subtract the “hot molecule” contribution to the molecular spectra. This is as simple as multiple Boltzmann distributions for different temperatures. Subtracting out the hot contribution would require absorption measurements to determine the number of molecules in the higher rotational states and using that as a determination of the hot temperature to

subtract its contribution to the overall spectra. For molecular systems that have several long lived rotational levels this effect is even more dramatic but in the first positive system of nitrogen this effect near thermal equilibrium of cryogenics should be non-negligible. Closer to lower temperatures, metastable transfer to nitrogen molecules would create a hot molecule contribution that is non-negligible as is seen in this work. Thus using the nitrogen ro-vibrational spectra as a thermometer in this work would be accurate provided absorption measurements are made which currently in the experimental setup it cannot be done. In order to measure accurately the hot molecule contribution the experiment would need additional optical quality windows to allow optical access to the jet so that a laser of wavelength matched to a molecular transition of higher energy than the first positive system could pass through the jet to measure the attenuation which in turn measures the number of molecules in those states brought there by metastable transfer instead of collisions from ground state neutrals. This is possible as optical windows on cryostats are not unreasonable.

3. MOLECULAR SPECTRA

The types of sources of spectral emission in atoms and molecules are electronic, vibrational, and rotational. Electronic transitions in molecules are perturbed by vibrational states which are on the order of 50 kJ/mol, and are characterized typically by dipolar interactions but can also be associated with higher order transitions. Rotational transitions are typically magnetic dipolar interactions which are dependent on rotational matrices. Higher order transitions use quadrupole interactions and so on. Transition probabilities are balanced when conditions for local thermodynamic equilibrium are reached, or when the kinetic temperature is approximately equal to the Planckian temperature. This means the rate of emission at a particular frequency, $R_{emission}(v)$, is proportional to the brightness or intensity of the emission at a temperature T and the constant of proportionality is due to absorption of the light at that frequency [63].

$$R_{emission}(v) = k_{absorption}(v) \times Brightness(T) \quad [17]$$

Local thermodynamic equilibrium conditions for each emitting rotational state are such that each level distribution is in thermal equilibrium so that the distribution can be considered as Boltzmann-like. The equilibrium temperature must be such that other non-emitting de-excitation processes are also balanced with emitting processes. There must also be a balance between the rotational

temperature of an emitting electronic state and the ground electronic state. The rotation-translation relaxation time should be shorter than the primary de-excitation process. This restriction allows for calculations known as “detailed balance” between states which was first theorized by Boltzmann in his great publication of 1872 [64].

3.1 Rotational perturbations

The intensity of spectral lines is given by the relationship between the population rate and the rate of absorption. Absorption is usually left in terms of an “interaction” operator which in general is a tensor but for the dipole case can be written as a two-dimensional matrix, $\hat{\mu}_{fi}$.

$$Intensity \propto \int_{All\ space} \psi_f \hat{\mu}_{fi} \psi_i d\tau \qquad [18]$$

$$B = \frac{\left|\hat{\mu}_{fi}\right|^2}{6\ \varepsilon_o \hbar^2} \qquad [19]$$

$$W = (N - N')B\rho \qquad [20]$$

The first rotational coefficient, *B,* is directly related to the interaction operator or as written is the dipole matrix. This is commonly how the strength of the interaction is measured. The rate of emission, *W*, is defined in terms of the rotational coefficient as shown.

Dipolar transitions are initially approximated by the “rigid rotator” model and this model works well with diatomic molecules. In general the expression for the moment of inertia is complex but symmetry can reduce it to three moments, and for a linear molecule reduces further to just one moment of inertia, as denoted as capital i and an index indicating the direction of each moment.

$$I_c \;\geq\; I_b \;\geq\; I_a \qquad [21]$$

$$I_c \;=\; I_b,\; I_a \;= 0 \qquad [22]$$

Rotational energy is classically related to the exchange in energy between moments of inertia. Quantum mechanically it is related to integral jumps between energy states and the solution to the Hamiltonian which is essentially replacing the angular momenta with operators, i.e. $H\Psi = \frac{L^2}{2I}\Psi = \frac{J(J+1)\hbar^2}{2I}\Psi$, where *J* is the rotational angular momentum quantum number.

$$Classical \begin{cases} E = \frac{1}{2}[I_c\omega_c^2 \;+\; I_b\omega_b^2] \\ E = \frac{1}{2}\left[\frac{\mathrm{J}_c^2}{I_c} + \frac{\mathrm{J}_b^2}{I_b}\right], J = I\omega \\ \mathrm{J}^2 = \mathrm{J}_a^2 + \mathrm{J}_b^2 + \mathrm{J}_c^2 = \mathrm{J}_b^2 + \mathrm{J}_c^2 \end{cases} \qquad [23]$$

$$Quantum\begin{cases} E(\mathrm{J}) = \mathrm{J}(\mathrm{J}+1)\hbar^2/2I \\ \mathrm{J}^2 = \mathrm{J}(\mathrm{J}+1)\hbar^2 \end{cases} \quad [24]$$

Without a change in energy there can be no light and the wavelength of light emitted is due to the difference in energy between levels involved. In this case the quantum is manifested as the integral numbering of energy levels or the quantization of angular momentum which is why the rigid rotor model is used because it is the simplest system of angular momentum. The total energy for each level can be written as a sum of electronic, $G(v)$, and rotational energy or $F_v(\mathrm{J})$.

$$E(v, \mathrm{J}) = G(v) + F_v(\mathrm{J}) \quad [25]$$

$$F_v(\mathrm{J}) = \frac{E(\mathrm{J})}{hc} = \frac{\mathrm{J}(\mathrm{J}+1)h}{8\pi^2 cI} = B[\mathrm{J}(\mathrm{J}+1)] \quad [26]$$

$$B = 2.787 \times \frac{10^{-46}}{I(kg \cdot m^2)} \quad [27]$$

$$B = 16.859/I\left(\mu_u \cdot \text{Å}^2\right), \quad [28]$$

where this is still for the linear molecule case and B is still referred to as the rotational parameter or the first order correction term. Corrections are often needed for higher order effects and are typically represented in a Taylor expansion. First order corrections are sometimes all that is needed to show that a theoretical expression of a physical phenomenon is to be trusted. Exceptions to this are abundant though they may not be immediately obvious. Einstein's field equations as applied to planetary motion are a demonstration of how the first order accuracy can be inaccurate without including higher order terms. A more specific example is the famous correction to the orbit of Mercury, which was not fully understood until Einstein came along and was not predictable without a constant "calibration" that Newton had described as some unseen higher power coming in and changing the orbit every so often. Einstein's second order field equations produce three components of the Γ_{44}^{σ} gravitational field that by symmetry reduce to a single parameter. This theoretical practice is not much different from applications to the rotation of molecules. Furthering the model to include correction terms is likened to using a massless spring model attached to a rotor, or the "non-rigid" rotor which is often the name referred to when discussing higher order corrections. In general it is expected that the moment of inertia increases with increased rotation and so the correction term should decrease the energy of the first order terms. Therefore for the linear case the correction term should have a leading negative sign. The rotational energy can then be written with such a correction term:

$$F(\mathrm{J}) = B[1 - u\mathrm{J}(\mathrm{J}+1)]\mathrm{J}(\mathrm{J}+1),\ u \ll 1 \qquad [29]$$

Upon separating the quadratic terms, it is rewritten as:

$$F(\mathrm{J}) = B\mathrm{J}(\mathrm{J}+1) - D\mathrm{J}^2(\mathrm{J}+1)^2,\ D \ll B \qquad [30]$$

The D parameter is referred to as the “anharmonic term” which is the first “correction” or the next term in the expansion for the rigid rotor model. Determining the rotational constant experimentally allows for a calculation of the bond length because the allowed transitions will be spaced at intervals of 2B which is inversely proportional to the square of the bond length.

Due to the conservation of angular momentum, the axial symmetry of the internal electric field conserves the projection of orbital angular momentum along the axis of symmetry. Quantized electronic states must therefore be degenerate in the total spin of all the electrons, so that the diatomic molecule electronic states are 2S + 1 degenerate.

For the $^3\Pi$ state, S = 1, and so there are three states, $^3\Pi_0$, $^3\Pi_1$, and $^3\Pi_2$ as shown in the following figure (3.1) which depicts the projection of orbital angular momentum along the axis of symmetry of a diatomic molecule.

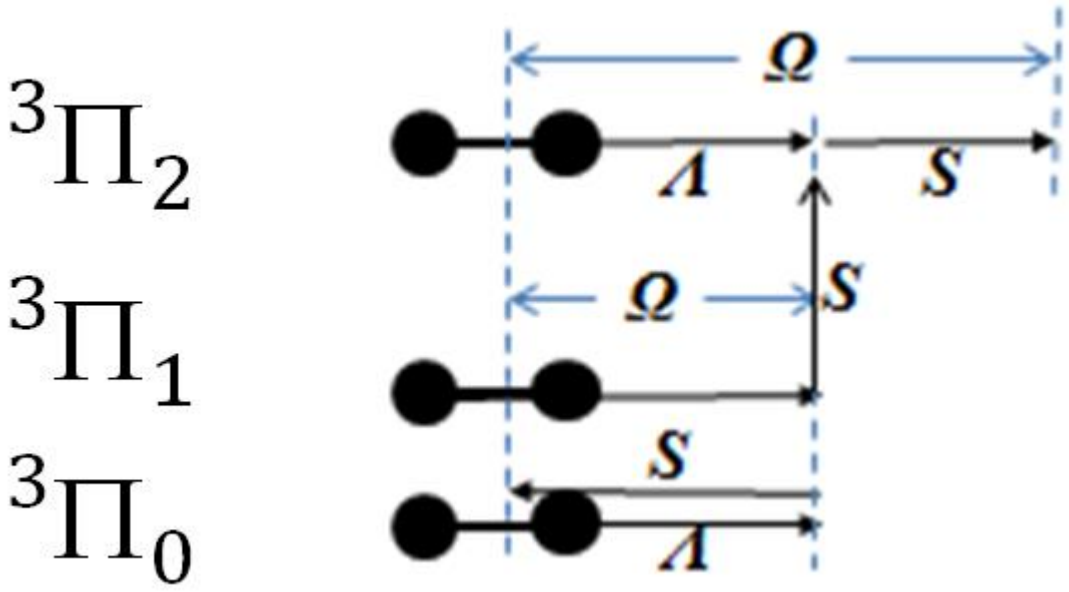

FIGURE
Figure 3.1: Vector diagram of spin and angular momentum of the 3-pi states. Directions of spin and orbital angular momentum of a diatomic molecule along the axis of symmetry are indicated.

The conserved quantity (labelled Ω) is the projection of the angular momentum operator along the axis of symmetry. Qualitatively this resembles the spin and orbital angular momentum of the electron in hydrogen. The quantized states of L and S that form the total angular momentum J are practically the same as the Λ and S that form Ω respectively. Just as for hydrogen, different values of Λ and S require the values of Ω to fall into conical sections if plotted together in three dimensions in analogy to J in the atomic hydrogen case.

3.2 Hund's cases

There are different cases for which rotational motion is coupled to the electronic motion, referred to as "Hund's cases" in which different observed phenomena in the spectra are observed. The first case, case (a), is the case where the interaction of electronic motion, spin and orbital, with nuclear rotation is weak but it is coupled strongly to the inter-nuclear axis. The geometry of the motion is like that of a symmetric top. This leads to a splitting of levels as a function of the total orbital angular momentum of the electron. The values for L and S combine to make J that is a cone with axis of symmetry that coincides with the perpendicular projection of angular momentum from the axis of symmetry, N.

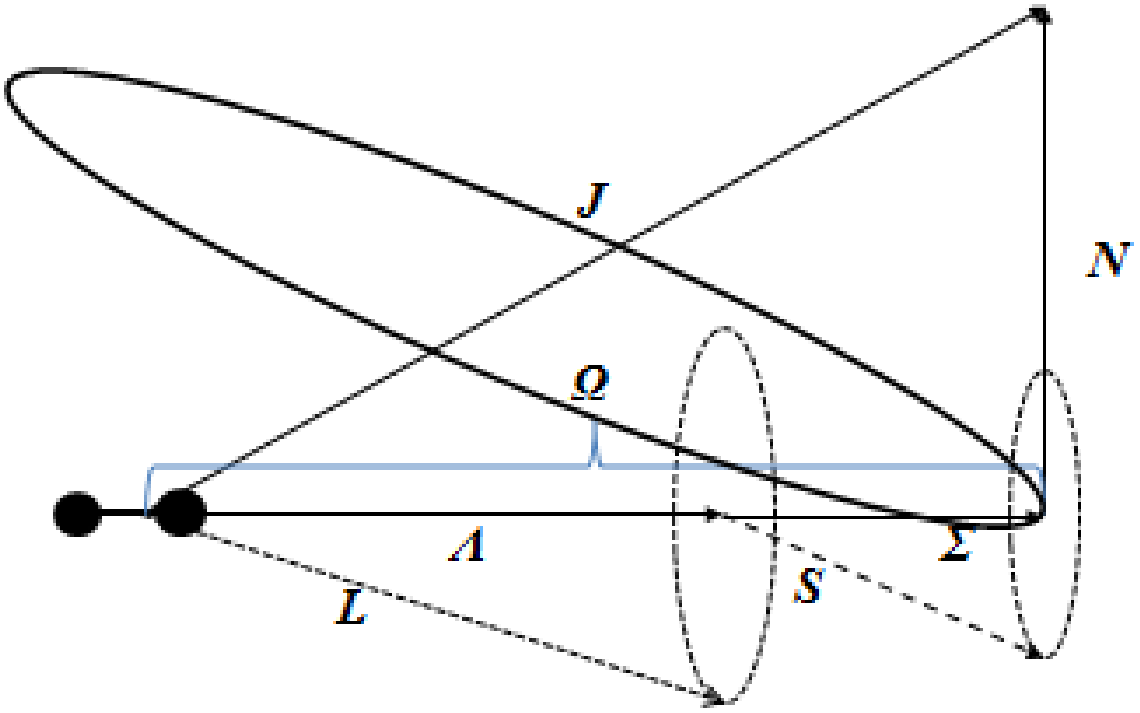

FIGURE
Figure 3.2: Vector diagram of the angular momenta for Hund's case (a) showing both the projection along the internuclear axis (Ω) and the normal component (N).

The second case, case (b), is where there is weak coupling of the spin to the inter-nuclear axis. It is during this case that the angular momentum Λ and N form a resultant vector K which is the total angular momentum without the spin angular momentum part. The quantum number for K can take on integral values starting from Λ stepping up by values of one. As shown in the figure if $\Lambda = 0$ then K would be the same as N and would be perpendicular to the axis of symmetry. Both vectors of angular momenta K and S will form a resultant J that can take on values from K + S to decreasing values by one until it equals the difference |K-S| and thus an additional 2S + 1 degeneracy is introduced and therefore the multiplicity is increased. It should be noted that by inspection both case (a) and case (b) are identical for *singlet* states because $\Lambda = \Omega$ and $K = J$, which means both cases are just the symmetrical top model in the previous figure. Similarly it should be obvious that Σ states will belong in case (b) always, and even for $\Lambda = 0 \text{ and } S \neq 0$, states the Hund's case (a) does not apply because the spin vector is completely uncoupled from the internuclear axis.

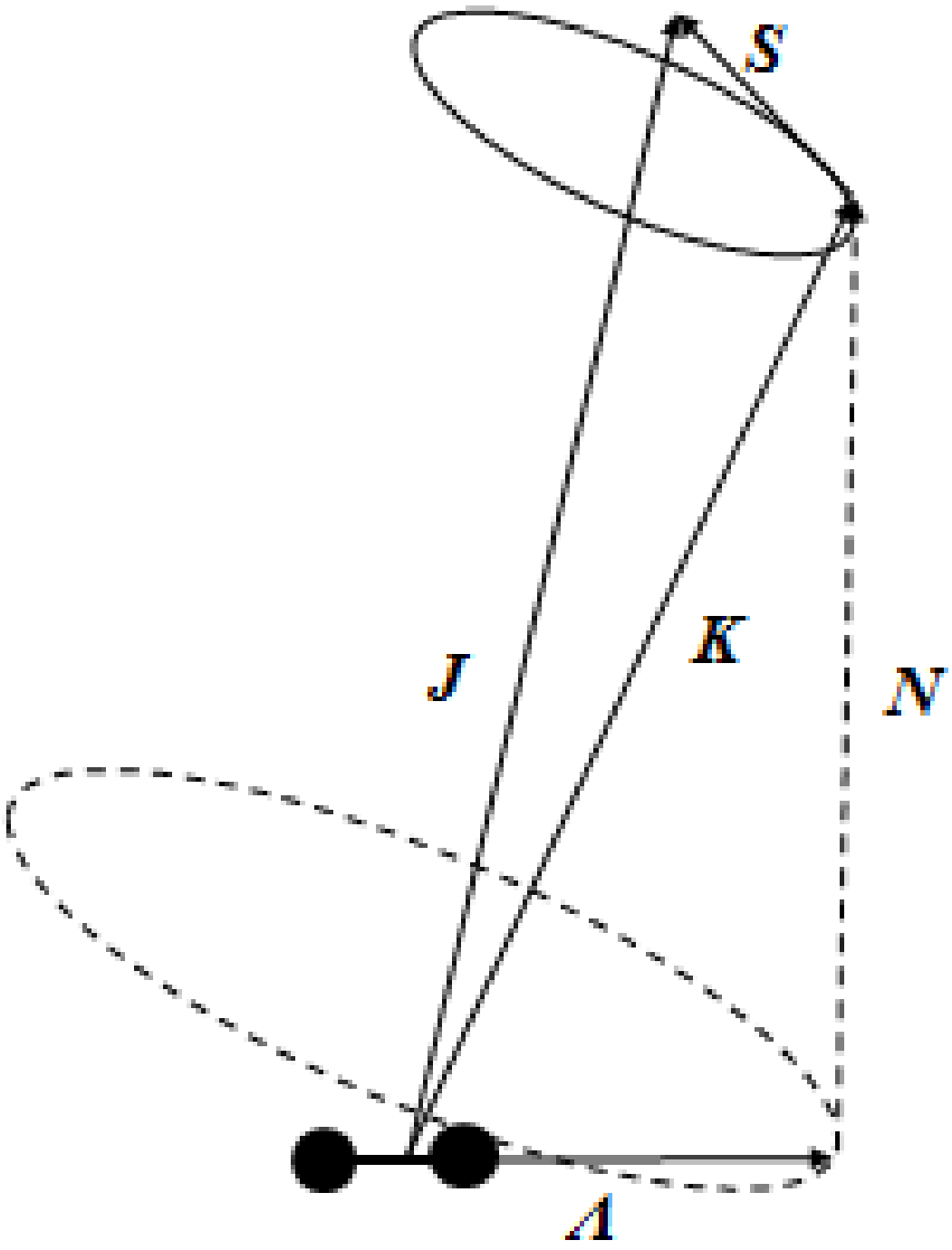

FIGURE
Figure 3.3: Vector diagram of angular momenta for Hund's case (b)

This is also true for light molecules, and even if $\Lambda \neq 0$, S may only be lightly coupled to the internuclear axis which is the notable characteristic of Hund's case (b). Multiplet states are usually found somewhere between cases (a) and (b) because they have a finite coupling strength of the spin to the internuclear axis which is expected for cold molecular gases.

3.3 Spin coupling strength

The strength of the coupling is dominated by the magnetic field that precesses with S and is proportional to Λ. The induced magnetic moment has a projection in the magnetic field direction that is proportional to Σ, the projection of the spin vector along the internuclear axis. Therefore the total electronic contribution to the magnetic field is given by equation 31.

$$T_e = T_0 + A\,\Lambda\Sigma \qquad [31]$$

The coupling constant, A, is unique to each multiplet, and it determines the magnitude of the splitting or energy difference between levels which increases with an increased number of electrons, as in the corresponding case with atoms. This coupling constant can be positive or negative which respectively generates *normal* or *inverted* terms. The result is an alternating multiplicity or degeneracy. Molecules with an even number of electrons will have *odd* multiplicities, since 2S+1 is odd, such as singlets and triplets, since *S* is integral. However, molecules with odd numbers of electrons have *even*

multiplicities which result in doublets, quartets, etc. since *S* will be half integral and 2S+1 is even. As J increases, S becomes further decoupled from the internuclear axis and thus reducing A. Therefore larger rotation would mean smaller splitting. The amplitude of the splitting, or the energy difference between levels, is determined by the ratio of coupling constant A and the rotational constant B, or Y = A/B. Therefore the effect of spin uncoupling is that the effective rotational parameter must include one constant, for the case of $\Sigma = 0$, and then include a first order correction term, for cases $\Sigma \pm 1$, and so on for higher order terms.

3.4 Symmetry

With all the quantum numbers introduced previously it would be useful to take a quick qualitative discourse about symmetry properties of the electronic eigenfunctions of molecular states. In diatomic molecules, and also in other linear molecules, any plane that includes the inter-nuclear axis will be a plane of symmetry. This results in non-degenerate states, such as sigma states, that are left with the preceding sign unchanged or changed for the electronic eigenfunctions when they have undergone reflection at any plane that includes both nuclei. For the pi states discussed earlier that will be used to discuss the states of nitrogen under study in this experiment, there is a small splitting that arises because for degenerate states the eigenfunction can overlap another eigenfunction during a symmetry operation, so therefore unchanged or changed sign eigenfunctions will result, but these can be written as a linear combination

of both the + or unchanged, and the – or changed sign eigenfunctions in what follows.

$$\varphi_e = a\varphi_e^+ + b\varphi_e^- \qquad [32]$$

It is because of this that there exist two eigenfunctions with the split being associated with the energy difference between each changed or unchanged eigenfunction. The rotation of the molecule therefore takes place with different energies, and the rotations of the electrons will contain both properties, since each eigenfunction, either φ_e^+ or φ_e^-, will include both $e^{+i\Lambda\varphi}$and $e^{-i\Lambda\varphi}$.

In the case of two nuclei having the same amount of charge and even if they have different masses (say for example $^{14}N^{14}N$ or $^{14}N^{15}N$), the field that the electrons experience will now have a center of symmetry which breaks the symmetry down to where the electronic eigenfunctions will remain with either an unchanged or a changed sign when the plane of reflection is at the center. In other words, the field $|\Psi|^2$ remains unchanged by a reflection of the nuclei through the center of symmetry and now cannot remain the same unless the symmetry operation includes this point. This is like a center of mass; the coordinates can now have a common origin that can be reflected, so that the only change being the sign change which would occur when the coordinates are inverted through this origin. As stated before, there will be fewer allowed symmetry operations. The case where the eigenfunctions are left unchanged is

called an *even* state and just as before the states with changed sign are *odd* states. The effect is the same even if dealing with degenerate or non-degenerate states. For the task of labelling states, this symmetry is labelled in states by adding a subscript a *g* or *u* referring to “gerade” or “ungerade” and note that electron spin should have no influence on this symmetry so all the components of a given multiplet will be even (*g*) or odd (*u*) due to this effect. One additional detail to point out is that this symmetry does not require the molecule to be homonuclear just as long as the charge is the same and this property is observed even with molecules of atoms that differ by one unit of charge since they closely resemble a molecule with this symmetry much like hydrogen-like atoms behave like hydrogen. As a consequence of this symmetry, there is an additional selection rule for transitions which is that even electronic states can combine (or overlap their wave function) only with odd states, which means transitions will proceed from $g \leftrightarrow u$ or vice versa but not the same symmetry for both the starting and ending state of the transition. This follows from the concept that symmetric states cannot overlap with anti-symmetric states of atoms.

3.5 Nitrogen first positive system

Can the nitrogen ro-vibrational spectrum be used as a thermometer? This work was carried forth under the proposition that the first positive system of molecular nitrogen emission spectrum can be used to determine the temperature of the jet and ultimately the sample region in situ. The addition of nitrogen to helium admixtures can be used to determine the mixture relative

density without affecting the emission of the system as discussed previously. The first positive system is readily accessible by electron impact because of the low threshold energy required to populate the upper states. It exhibits multiple-headed bands degraded to shorter wavelengths and has a wide range from infrared to blue wavelengths. Figure (3.4) shows the bands resulting from vibrational levels between the $B^3\Pi_g \rightarrow A\ ^3\Sigma_u^+$ electronic levels. The spin-orbit constant for the upper state is ~42 cm^{-1} while the rotational parameter is somewhere between 1.63 cm^{-1} and 1.59 cm^{-1} depending on the branch such that the strength of coupling parameter Y = A/B is ~26. Therefore it is a very good approximation to treat the upper state as purely Hund's case (a) for low values of J. The availability of low-lying states also makes nitrogen a great addition to graphene-like nano-tubes to increase the electrochemical activity without appreciable change to its electric conductivity [65]. Electron impact, although messy in the sense that it doesn't select the final excited state, can proceed across spin forbidden transitions [66]. The dipole-allowed transitions from the ground state $X^1\Sigma_g^+$ to $^1\Sigma_u^+$ and $^1\Pi_u$ have transition frequencies in the extreme ultraviolet (XUV) range which is one mechanism that protects the Earth's surface from XUV solar radiation via absorption by nitrogen in the atmosphere. Other de-excitation processes have transition probabilities that are at least one order of magnitude smaller than the emission processes of the first positive system of nitrogen. Rotational coupling causes the state $B^3\Pi_g$ to have three sub-bands, one for each spin, and in each state are nine branches, three

for each triplet of the lower state, which means there are in total 27 branches for the system we are studying in this work. One reason to use the first positive system as a thermometer is that the radiative lifetime is long, between 12-14 microseconds, which provides for rotational-translational equilibration at pressures as low as 10 millitorr. This system has been extensively studied for many different molecules but for specifically nitrogen it was the work of Naudé that measured the spectrum of the $B^3\Pi_g \rightarrow A\ ^3\Sigma_u^+$ for Hund's case (a) [67]. Note that for Hund's case (b) the selection rules discussed previously would require $\Delta K = 0, \pm 1$, and transitions where $\Delta K \neq \Delta J$ would be weak and would be missing from the spectrum. Recall that K is the total angular momentum minus the spin angular momentum when it is decoupled as shown in figure (3.3). Therefore, if the case were case (b), only nine branches would be present in the spectrum corresponding to $P_{11}, Q_{11}, R_{11}, P_{22}, Q_{22}, R_{22}, P_{33}, Q_{33}, \text{and } R_{33}$ with any appreciable intensity and the other branches would be vanishingly small. The measured spectra in this work had always shown all the branches. At low temperatures the spin should be strongly coupled to the internuclear axis and so it would be a surprise to see anything other than case (a) and no decoupling observed.

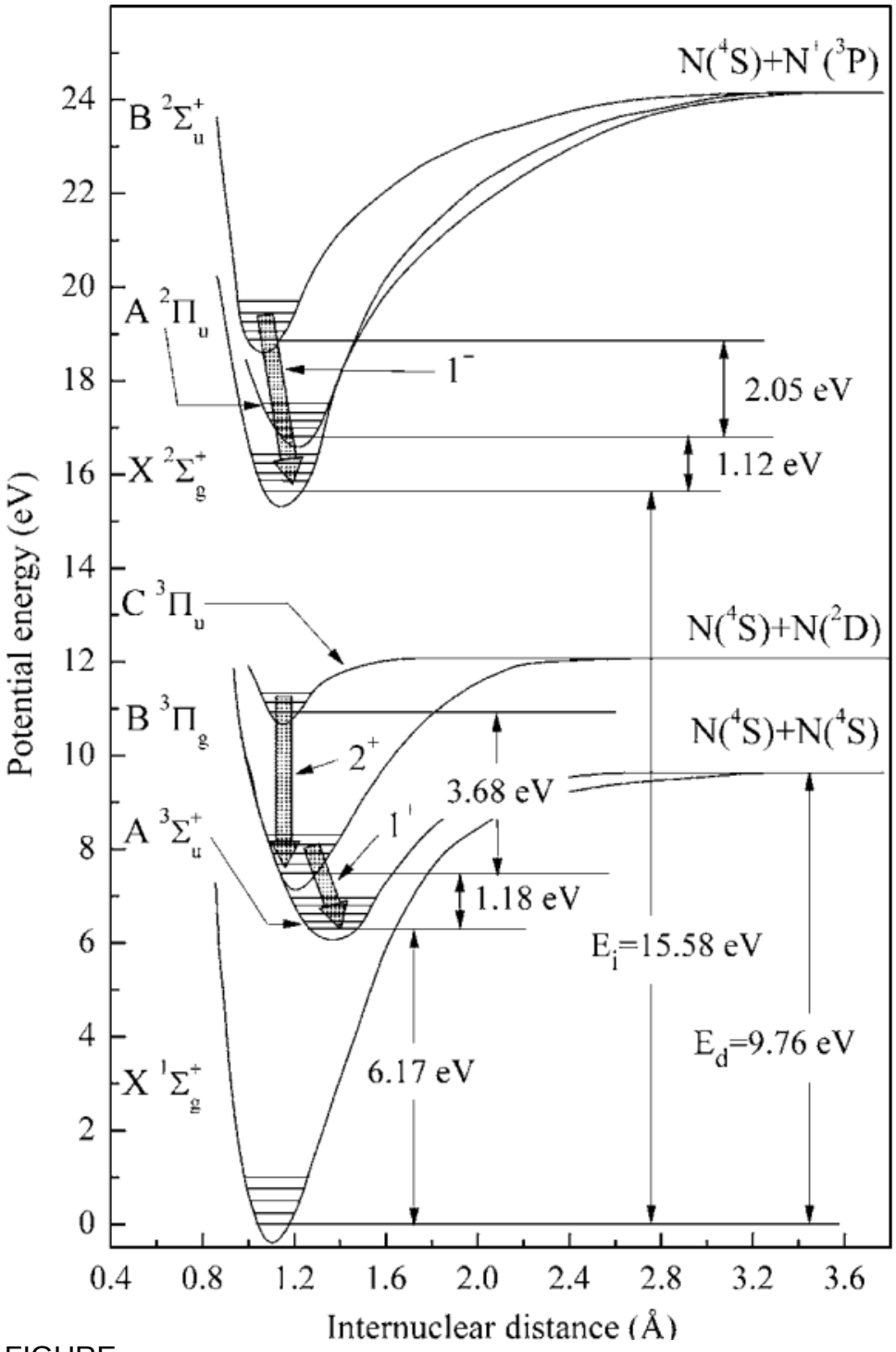

FIGURE

Figure 3.4: Potential energy curves for diatomic nitrogen. The first and second positive systems are indicated as bold arrows along with the first negative system. Reprinted with permission from [68].

It is expected that the intensity distribution of rotational lines is proportional to measured intensity. During thermodynamic equilibrium the distribution of states is given by the Boltzmann factor and a constant of proportionality that includes a degeneracy term. Thus the task of finding the temperature can be reduced to finding a linear relationship between temperature and measured intensity by taking the natural logarithm of both sides, as shown below.

$$P \propto I \propto \frac{g}{Z} \times exp(-E_{rot}hc/kT_{rot}) \quad [33]$$

$$log(I) = const - E_{rot}hc/kT_{rot} \quad [34]$$

Therefore a rotational temperature can be found with a prior knowledge of the energies of the levels and a measured intensity distribution. The leading constant, that depends on spin, which accounts for degenerate states that pile up on the same energy, is readily seen in data sets. This can be identified by alternating intensities in the measured distribution that would lead to identical slopes but shifted y-intercept, for the logarithm of intensity axis, in the log-linear extrapolation mentioned in equation 34.

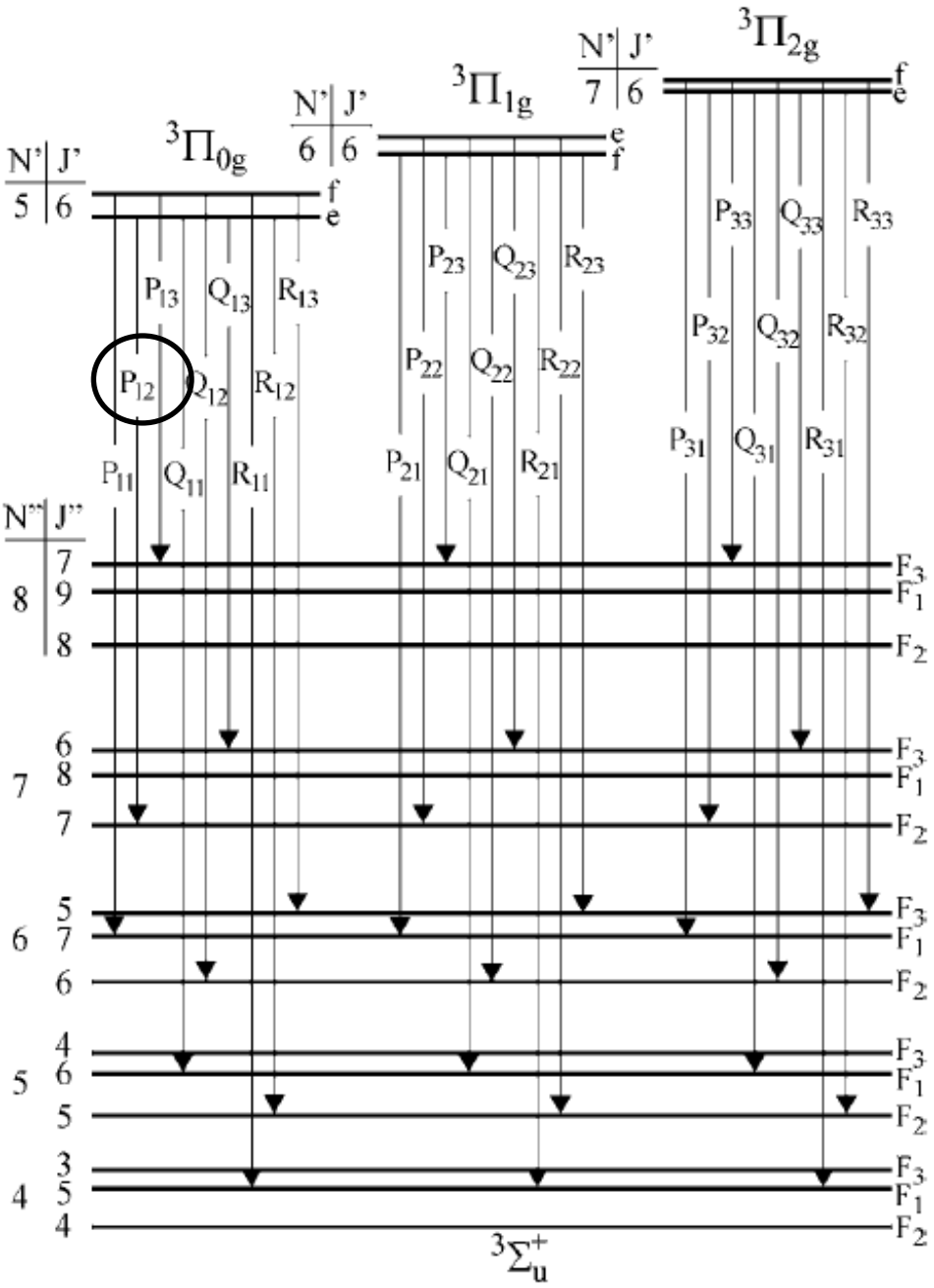

FIGURE

Figure 3.5: Energy level scheme for the first positive system of nitrogen depicting the P, Q, and R branches for Hund's case (a). The rotational temperature analysis done in this work used the P_{12} branch as indicated. The e/f indicate parity of the states. Reprinted with permission from [68].

Normally, without spin degeneracy you would see clean peaks that follow a continuous Poissonian curve envelope. In the case of this work, an alternating intensity of two envelopes was observed, one of higher intensity than the other as shown in figure (3.6). These alternating intensity peaks are due to symmetric and antisymmetric states.

Figure (3.6) shows the P and Q R branches of the v'=2, v = 0 system of P_{12} in the first positive system of Nitrogen as measured in this experiment. As can be seen in the energy diagram for the first positive system of nitrogen in figure (3.5), the upper state is singlet and the lower state is triplet, indicated by the F_1, F_2, and F_3 energy values. It is one of several high resolution spectra taken using the Andor spectrometer system in this work. The largest intensity states are symmetric states due to degeneracy and the lower intensity are antisymmetric as governed by the transition rules, $\Delta\Lambda = -1$. It is worth noting that the Λ quantum number is the projection of the orbital angular momentum along the axis of symmetry and this rule is very similar to the rules for L in the hydrogen atom as discussed earlier.

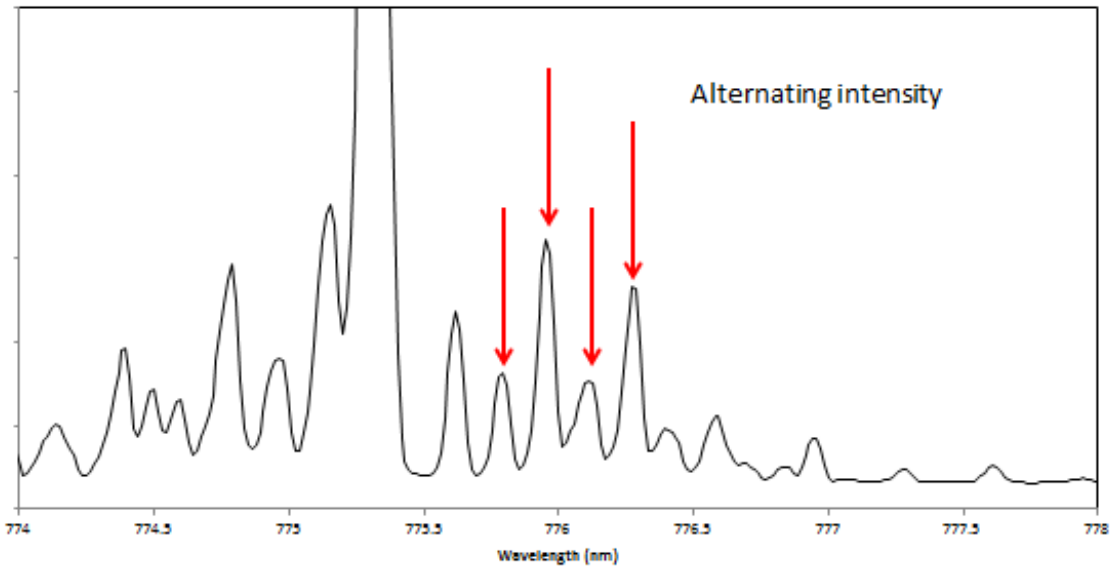

FIGURE
Figure 3.6: High resolution data of the P_{12} branch of the first positive system of nitrogen with alternating intensities shown by arrows.

Since the final state is singlet and the initial state is triplet for the transition there are two symmetric states that overlap and one antisymmetric that does not. Therefore including symmetry in the leading constant for the intensity distribution, $\Phi_{J'} =$ 2/3 for symmetric and 1/3 for anti-symmetric. The full spin term is referred to as the Hönl-London factors, S_J^P [69].

$$I = const \times \Phi_{J'} \times S_{J'}^P \times exp(-E_{rot} hc/kT_{rot}) \quad [35]$$

$$S_{J'}^P = \frac{(J' + 1 + \Lambda')(J' + 2 + \Lambda')}{4(J' + 1)} \quad [36]$$

3.6 Nitrogen thermometry

The study of rotational temperature of nitrogen in the jet did provide a thermometer for the temperature of the jet. As expected with such a large aperture for the fiber it is mostly measuring an average. The fiber optic height in relation to the jet was adjusted and found to decrease with temperature as expected for a lower temperature at the surface of superfluid helium relative to the temperature at the exit of the jet into the helium environment. As seen in figure (3.7) there appears to still be an overlapping trend that almost seems to be sinusoidal around the straight line fit. The appearance of this trend is common in ionic gases where there is a separate temperature for the electrons

and the ions because of the mass difference between electrons and nuclei, and where the two distributions almost never reach equilibrium [70].

In the jet there are multiple excitation mechanisms of nitrogen molecules, some are excited by metastable helium and others through recombination processes or even collisions with other excited nitrogen molecules. However, it is expected that all the excitation processes originate from the ground molecular state and so it would be expected that using a thermodynamic equilibrium model would work with only one temperature. What is happening is a competition between processes and the rotational temperature is only equal to the gas temperature when the rotation-translation relaxation time is much less than the radiative lifetime of the states used in the temperature determination. The recombined molecules will have had enough time to relax to their ground state whereas molecules that have been involved in collisions with helium will have altered temperatures of rotation due to the high energy transfer with metastable helium and few other collisions. The result would be two distributions and the straight line fit would be superimposed with another slope, due to metastable transfer and hence the apparent departure from the straight line fit in figure (3.7).

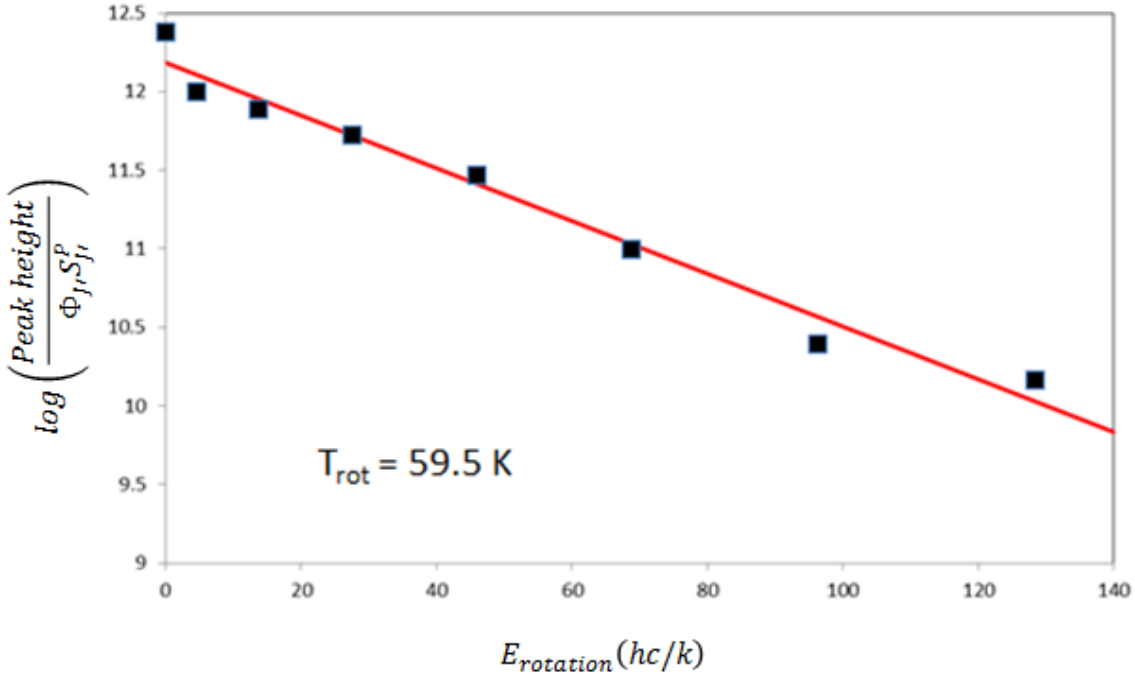

FIGURE

Figure 3.7: Linear fit taken from high resolution spectra of the first positive system of nitrogen. Each point represents a peak in the spectrum. Rotational temperature is indicated as found from the slope of the linear fit. One “knee” is clearly seen while a second could be inferred with increasing energy of rotation.

4. PERTURBATIVE METHOD FOR ROTATIONAL LEVELS

The rotational levels are found through perturbation theory. To begin with it is usually customary to write the Hamiltonian of the system in two parts:

$$\hat{H} = \hat{H}_o + \hat{H}_p \qquad [37]$$

where the first term is assumed to have known eigenvalues and eigenfunctions and the second term is the perturbation Hamiltonian. By using the properties of the unperturbed system the eigenfunctions and eigenvalues of the total Hamiltonian can be found:

$$\hat{H}|n\rangle = \xi_n|n\rangle \qquad [38]$$

The way to proceed is to take a power series of matrix elements of $\hat{H}_p$, Schrödinger originally gave the first and second order terms explicitly [71]. The calculation was extended by Condon and Shortley who found a procedure to obtain all the higher-order terms. [72] There is, however, a simpler method to obtain a series correct to the fifth order and with little more effort correct to seventeenth order but in this and most calculations, third-order terms are sufficient. [73]

In the case of molecules, the unperturbed Hamiltonian is divided into $\hat{H}_o = \hat{H}_{el} + \hat{H}_R$, electronic and rotational respectively, which consists of the non-

relativistic motions of electrons and nuclei. Starting with the assumption that the eigenvalues and eigenfunctions of $\hat{H}_o$ are known, which is not true actually since the eigenvalue problem is very complicated and only solved for some special cases, and for others even with modern computational physics techniques it remains to be solved. However, empirical data from spectroscopic observations can determine which of the eigenvalues would arise from an adiabatic potential, U_n, but not provide much information about the eigenfunctions themselves. In spite of all this, perturbation theory can provide a means to determine experimental values that follow from the perturbation formulae. In terms of the philosophy of the method, all physics can be considered as a perturbation theory, because observations are made up of perturbations between the observer and that which is produced by physical instrumentation.

4.1 First order

To first order the Hamiltonian matrix can be found by assuming that the eigenkets of $\hat{H}_o$ form a complete orthonormal set. These will be used to construct a basis for which the corresponding matrix will have diagonal elements of the form $\xi_n^{\,o} + \langle n^o|\hat{H}_p|n^o\rangle$ and the non-diagonal elements will only involve perturbation terms. By adding a diagonal matrix of -λ and taking the determinant of the new matrix and equating it to zero, one finds the secular equation for the eigenvalue problem. The determinant can be expanded so that each diagonal element appears as a pair such that $\langle m^o|\hat{H}_p|n^o\rangle\langle n^o|\hat{H}_p|m^o\rangle$ or in higher order products of $\hat{H}_p$. Hence the secular equation can be written as

$$\left(\xi_n{}^o + \langle n^o|\hat{H}_p|n^o\rangle - \lambda\right)\left(\xi_m{}^o + \langle m^o|\hat{H}_p|m^o\rangle - \lambda\right)(\ldots - \lambda) + O\left(\hat{H}_p{}^2\right) = 0 \quad [39]$$

The first term is the product of all diagonal elements, and the next term contains all other terms in which non-diagonal elements will appear such that if $\xi_n{}^o$is different from the zeroth-order eigenvalue, the correction term is given by:

$$\xi_n{}^{(1)} = \xi_n{}^o + \langle n^o|\hat{H}_p|n^o\rangle \quad [40]$$

which is an eigenvalue to first order in $\hat{H}_p$ since we've assumed there is no degeneracy and all factors are of the order of $\hat{H}_p$.

Before discussing the degenerate case it would probably be a good idea to give a short primer on the space contraction operator and also prior to the third order perturbation theory. The space contraction operator is an operator that parameterizes the space based on the assumption that the full Hermitian plus perturbation is unitary and the operator is defined by:

$$\hat{S}_n{}^0 = \hat{I} + \left(\xi_n{}^o - \hat{H}_o - \hat{Q}_n\hat{H}_p\right)^{-1}\hat{Q}_n\hat{H}_p \quad [41]$$

Where $\hat{I}$ is the identity unit operator and

$$\hat{Q}_n \equiv \hat{I} - |n^0\rangle\langle n^0| \qquad [42]$$

Then the denominator of the space contraction operator can be rewritten as:

$$\begin{aligned}
\left(\xi_n{}^o - \hat{H}_o - \hat{Q}_n\hat{H}_p\right)^{-1} &= \left(\xi_n{}^o - \hat{H}_o\right)^{-1}\left(\xi_n{}^o - \hat{H}_o\right)\left(\xi_n{}^o - \hat{H}_o - \hat{Q}_n\hat{H}_p\right)^{-1} \\
&= \left(\xi_n{}^o - \hat{H}_o\right)^{-1}\left(\xi_n{}^o - \hat{H}_o - \hat{Q}_n\hat{H}_p + \hat{Q}_n\hat{H}_p\right)\left(\xi_n{}^o\right. \\
&\left. - \hat{H}_o - \hat{Q}_n\hat{H}_p\right)^{-1} \\
&= \left(\xi_n{}^o - \hat{H}_o\right)^{-1}\left[1 + \hat{Q}_n\hat{H}_p\left(\xi_n{}^o - \hat{H}_o - \hat{Q}_n\hat{H}_p\right)^{-1}\right] \\
&= \left(\xi_n{}^o - \hat{H}_o\right)^{-1} \\
&+ \left(\xi_n{}^o - \hat{H}_o\right)^{-1}\hat{Q}_n\hat{H}_p\left(\xi_n{}^o - \hat{H}_o\right)^{-1} + \ \ldots
\end{aligned} \qquad [43]$$

Therefore the space contraction operator can be expressed as an infinite power series of $\hat{Q}_n\hat{H}_p$ as follows:

$$\begin{aligned}
\hat{S}_n{}^0 &= \hat{I} + \left(\xi_n{}^o - \hat{H}_o\right)^{-1}\hat{Q}_n\hat{H}_p\hat{S}_n{}^0 \\
&= \hat{I} + \left(\xi_n{}^o - \hat{H}_o\right)^{-1}\hat{Q}_n\hat{H}_p\left(\xi_n{}^o - \hat{H}_o\right)^{-1}\hat{Q}_n\hat{H}_p + \ \ldots
\end{aligned} \qquad [44]$$

Now using the transformation $|n^0\rangle \rightarrow \hat{S}_n{}^0\,|n^0\rangle$ one can write:

$$\begin{aligned}
\left\langle n^0\middle|\hat{S}_n{}^{0\dagger}\hat{S}_n{}^0\ \middle|n^0\right\rangle &= 1 + \left\langle n^0\middle|\hat{S}_n{}^{0\dagger}\,\hat{Q}_n\hat{H}_p\left(\xi_n{}^o - \hat{H}_o\right)^{-2}\hat{Q}_n\hat{H}_p\,\hat{S}_n{}^0\ \middle|n^0\right\rangle \\
&= 1 + \sum_{m\neq n}\frac{\left|\left\langle n^o\middle|\hat{H}_p\middle|n^o\right\rangle\right|^2}{\left(\xi_n{}^o - \xi_m{}^o\right)^2} + \ \ldots
\end{aligned} \qquad [45]$$

Here the property $\hat{Q}_n|n^o\rangle = 0$ has been used, and also that both $\hat{Q}_n$ and $\hat{H}_p$ are Hermitian. Continuing a step further into simplification using this,

$$\langle n^0|\hat{S}_n{}^{0\dagger}\hat{S}_m{}^0\ |m^0\rangle = \frac{\langle n^o|\hat{H}_p|m^o\rangle}{\left(\xi_m{}^o - \xi_n{}^o\right)^2}\left(\langle n^o|\hat{H}_p|n^o\rangle + \langle m^o|\hat{H}_p|m^o\rangle\right) + \ \ldots \qquad [46]$$

The higher order terms are of order ${H_p}^3$ and above. Therefore we can write,

$$\langle n^0|\hat{S}_n{}^{0\dagger}\,\hat{H}\ \hat{S}_m{}^0\ |m^0\rangle = \frac{\langle n^o|\hat{H}_p|m^o\rangle}{\left(\xi_m{}^o - \xi_n{}^o\right)^2}\left(\xi_m{}^o\langle n^o|\hat{H}_p|n^o\rangle + \xi_n{}^o\langle m^o|\hat{H}_p|m^o\rangle\right) + \ \ldots \qquad [47]$$

where the higher terms are on the order of ${H_p}^3$ and above again. So when $\hat{S}_n{}^0\,|n^0\rangle,\ \hat{S}_m{}^0\,|m^0\rangle, \ldots$ are taken as bases for the calculation of the matrix $\hat{H} - \lambda\hat{I}$, the previous equations show that all the non-diagonal matrix elements are on the order of ${H_p}^2$ or higher, which means if you equate one of the elements to zero and you have no degeneracy

$$\xi_n{}^{(3)} = \frac{\langle n^0|\hat{S}_n{}^{0\dagger}\,\hat{H}\ \hat{S}_n{}^0\ |n^0\rangle}{\langle n^0|\hat{S}_n{}^{0\dagger}\hat{S}_n{}^0\ |n^0\rangle} \qquad [48]$$

which will be correct up to order ${H_p}^3$.

4.2 Third order

In the third order perturbation formula in equation 48, the denominator has already been found in 45. The numerator is calculated by using the following relationships of the contraction operator and the Hamiltonian.

$$\hat{H}\hat{S}_n{}^0\left|n^0\right\rangle = \xi_n{}^o\hat{S}_n{}^0\left|n^0\right\rangle + \left(\hat{1}-\hat{Q}_n\right)\hat{H}_p\hat{S}_n{}^0\left|n^o\right\rangle \quad [49]$$

$$\hat{S}_n{}^{0\dagger}\left(\hat{1}-\hat{Q}_n\right) = \hat{1}-\hat{Q}_n + \hat{S}_n{}^{0\dagger}\hat{H}_p\hat{Q}_n\left(\xi_n{}^o-\hat{H}_0\right)^{-1}\left(\hat{1}-\hat{Q}_n\right) = \hat{1}-\hat{Q}_n = \left|n^0\right\rangle\left\langle n^0\right| \quad [50]$$

Which then gives for the numerator of the energy eigenvalue:

$$\left\langle n^0\middle|\hat{S}_n{}^{0\dagger}\,\hat{H}\;\hat{S}_n{}^0\;\middle|n^0\right\rangle = \xi_n{}^o\left\langle n^0\middle|\hat{S}_n{}^{0\dagger}\hat{S}_n{}^0\;\middle|n^0\right\rangle + \left\langle n^0\middle|\;\hat{H}_p\;\hat{S}_n{}^0\;\middle|n^0\right\rangle \quad [51]$$

By inserting this result the third order energy eigenvalue can be found as

$$\begin{aligned}\xi_n{}^{(3)} &= \xi_n{}^o + \frac{\left\langle n^0\middle|\;\hat{H}_p\;\hat{S}_n{}^0\;\middle|n^0\right\rangle}{\left\langle n^0\middle|\hat{S}_n{}^{0\dagger}\hat{S}_n{}^0\;\middle|n^0\right\rangle} \\ &= \frac{(nn)+\sum_{m\neq n}[(nm)(mn)/m]+\sum_{m\neq n,l\neq n}[(nl)(lm)(mn)/lm]+\;\ldots}{1+\sum_{m\neq n}[(nm)(mn)/m^2]+\;\ldots}\end{aligned} \quad [52]$$

Where $(mn)\equiv\left\langle m\middle|\;\hat{H}_p\;\middle|n^0\right\rangle$ and $m=\;\xi_n{}^o-\xi_m{}^o$ for the numerator and denominator terms respectively.

When an approximation is given by a ratio of two power series, it is referred to as a "Padé approximant" [74] [75]. The last term in the third order eigenvalue is a Padé approximant in terms of $\hat{H}_p$ and when expanded in a single power series we get the result of the perturbation series up to third order. To first order this type of derivation is used primarily to solve for the upper limit of a lowest energy level. However, the larger expanded version of the series may

yield larger or smaller values for the energy and it cannot be determined which case it will be prior to calculation for it will oscillate around the energy level.

4.3 Degenerate case

Now to address the degenerate case because it is important in diatomic molecules and many other situations. Replace the projection operator with the Nth degenerate states in order to exclude all states in the degenerate space:

$$\hat{Q}_N = \hat{1} - |n_1{}^0\rangle\langle n_1{}^0| - |n_2{}^0\rangle\langle n_2{}^0| - \cdots - |n_N{}^0\rangle\langle n_N{}^0| \quad [53]$$

Also change the contraction operator for those states to:

$$\hat{S}_N{}^0 = \hat{1} + \left(\xi_n{}^o - \hat{H}_0\right)^{-1} \hat{Q}_N \hat{H}_p \hat{S}_N{}^0 \quad [54]$$

For states not in the degenerate space we obtain a similar secular equation:

$$det \begin{vmatrix} \left\langle n_1{}^0 \left| \hat{S}_N{}^{0\dagger} \left(\hat{H} - \lambda\right) \hat{S}_N{}^0 \right| n_1{}^0 \right\rangle \ldots \left\langle n_N{}^0 \left| \hat{S}_N{}^{0\dagger} \left(\hat{H} - \lambda\right) \hat{S}_N{}^0 \right| n_1{}^0 \right\rangle \\ \ldots\ldots\ldots\ldots\ldots\ldots\ldots\ldots\ldots\ldots\ldots\ldots\ldots\ldots\ldots\ldots\ldots\ldots \\ \left\langle n_1{}^0 \left| \hat{S}_N{}^{0\dagger} \left(\hat{H} - \lambda\right) \hat{S}_N{}^0 \right| n_N{}^0 \right\rangle \ldots \left\langle n_N{}^0 \left| \hat{S}_N{}^{0\dagger} \left(\hat{H} - \lambda\right) \hat{S}_N{}^0 \right| n_N{}^0 \right\rangle \end{vmatrix} \quad [55]$$

The solutions of this equation are correct up to the order of $H_p{}^3$. Then the terms of the secular equation are specifically $\langle n_i{}^0 | \hat{S}_N{}^{0\dagger} \hat{H} \hat{S}_N{}^0 | n_j{}^0 \rangle$ up to second order. Also replacing $\langle n_i{}^0 | \hat{S}_N{}^{0\dagger} \hat{S}_N{}^0 | n_j{}^0 \rangle$ with a Kronecker delta function δ_{ij}, gives the well-known result known as the *Van Vleck approximation*, even though Van Vleck never published the proof of it [76].

Some simplifications arise when applying symmetry and using the situation that the $^3\Pi$ states are usually in Hund's case (a) then knowing the splitting in energy from previous work, one can approximate the energy levels using specific cases. Looking at the case where the total spin of the electrons is zero one can write the electronic and nuclear angular momenta as a vector sum, i.e. $\vec{J} = \vec{L}_{elec} + \vec{L}_{nucl}$ for which the sum of the nuclear angular momentum along the inter-nuclear axis disappears so that $J_\Omega = \Lambda$. Using the dipole operator, the total electric dipole operator is then $d = d_{elec} + d_{nucl}$ and thus the probability for an electric dipole transition becomes n'J'Λ' $\rightarrow$ n"J"Λ" which is proportional to the square of the dipole matrix element.

$$|\langle n'J'\Lambda'|d|n"J"\Lambda"\rangle|^2 = S(J',\Lambda'|J",\Lambda")|\langle n'\Lambda'|d|n"\Lambda"\rangle|^2 \quad [56]$$

The quantity $S(J',\Lambda'|J",\Lambda")$ is the same Hönl-London factors discussed earlier and it contains all the information concerning the transition probability of the nuclear angular momentum. The importance of discussing this expansion should be clear now; it is where these factors come from. One should note that they are symmetric in (J', Λ') $\rightarrow$ (J", Λ"). The other quantity is the square of the matrix element of the dipole operator where the molecule is assumed to be stationary and, in the case that n'Λ' and n"Λ" are the same, this is the permament dipole moment of the molecule which points in the direction of the inter-nuclear axis.

Including the other spin terms as shown in the previous calculation would be simply to add a statistical weight. The probabilities are summed over upper and lower states so that to calculate the probability of emission all one would need is the 2J+1 factor for the upper state. The Hönl-London factors for $\Delta\Lambda$=0 are given (for the case of emission, written in terms of J' which is included in the Boltzmann-factor) [77]

$$S_{J'}^{R} = \frac{(J'+\Lambda')(J'-\Lambda')}{J'}$$

$$S_{J'}^{Q} = \frac{(2J'+1)\Lambda'^{2}}{J'(J'+1)} \qquad [57]$$

$$S_{J'}^{P} = \frac{(J'+1+\Lambda')(J'+1-\Lambda')}{J'+1}$$

For $\Delta\Lambda$ = +1

$$S_{J'}^{R} = \frac{(J'+\Lambda')(J'-1+\Lambda')}{4J'}$$

$$S_{J'}^{Q} = \frac{(J'+\Lambda')(J'+1-\Lambda')(2J'+1)}{4J'(J'+1)} \qquad [58]$$

$$S_{J'}^{P} = \frac{(J'+1-\Lambda')(J'+2-\Lambda')}{4(J'+1)}$$

For $\Delta\Lambda$ = -1

$$S_{J'}^{R} = \frac{(J'-\Lambda')(J'-1-\Lambda')}{4J'}$$

$$S_{J'}^{Q} = \frac{(J'-\Lambda')(J'+1+\Lambda')(2J'+1)}{4J'(J'+1)} \qquad [59]$$

$$S_{J'}^{P} = \frac{(J'+1+\Lambda')(J'+2+\Lambda')}{4(J'+1)}$$

The rotational parameters are related to the matrix elements of the rotational part of the Hamiltonian and using Hund's case (b) the basis functions are singlet states, $|\Lambda NM\rangle$, and so the most simple case is when spin is decoupled. The rotational part of the Hamiltonian in Hund's case (b) yields two types of matrix elements.

$$\begin{gathered}\hbar^2\hat{H}_{rot} = \hat{B}\left(\hat{N}^2 - \hat{N}_+\hat{L}_- - \hat{N}_-\hat{L}_+\right) \\ \langle \Lambda NM|\hat{H}_{rot}|\Lambda NM\rangle = B\{N(N+1) - \Lambda^2\} \\ \langle \Lambda \pm 1NM|\hat{H}_{rot}|\Lambda NM\rangle = -\langle \Lambda \pm 1|\hat{H}_{rot}|\Lambda\rangle\hbar^{-1}\sqrt{N(N+1) - \Lambda(\Lambda \pm 1)}\end{gathered} \quad [60]$$

The first result gives the diagonal matrix element and rotational parameter B. The D parameter is given by doing a Taylor series and applying the perturbation terms as discussed earlier.

4.4 Rotational levels and adiabatic potential

As mentioned previously, the result of the perturbation theory yields a Padé approximant of N(N+1) terms. There are multiple ways to connect the energy of rotational levels to experiment. One of the most common ways is by using the Born-Oppenheimer approximation or by assumption that the electronic states of the Hamiltonian are solved exactly and treat the rotational levels as perturbations. Experimental data is conventionally analyzed in terms of a Taylor series and so it is customary to express the energy in terms of a simple Taylor series of N(N+1) and that is the result as follows which was originally derived by Dunham [78]. First it is assumed that the adiabatic potential as a function of the distance between nuclei is a power series expansion.

$$U_n = hca_o\xi^2(1+a_1\xi+a_2\xi^2+a_3\xi^3+\cdots) \quad [61]$$

Where the difference between the radius and the equilibrium radius is included in the $\xi = \frac{R-R_e}{R_e}$ term and the series is about $\xi = 0$. Also $a_o = \omega_e/4B_e$; $\omega_e$is the classical frequency of small oscillations and $B_e = \frac{h}{(8\pi m r_e^2 c)}$ is the rotational parameter. Note that if all the coefficients are made equal to zero the potential becomes the simple harmonic oscillator potential. From this starting point Dunham made the assumption that all the coefficients are perturbation terms and therefore the corrections to the energy are given by steps along an oscillator potential.

$$F_{vN} = \sum_{l,j} Y_{lj}\left(v+\tfrac{1}{2}\right)^l [N(N+1)]^j \quad [62]$$

The first index for the coefficients Y_{lj} refers to the power of the vibrational quantum number and the second is the power of the rotational quantum number. This power series is also further made to resemble the harmonic potential by making it a series in the vibrational quantum number. Thus begins the connection between the perturbation theory and the experimental results as found by spectroscopists which prefer to use notation that resembles a Taylor series like expansion with coefficients referred to as “band spectrum constants” which today are the most frequently used to describe rotational energy spectra.

$$F_{vN} = \omega_e\left(v+\tfrac{1}{2}\right) - \omega_e x\left(v+\tfrac{1}{2}\right)^2 + \omega_e y\left(v+\tfrac{1}{2}\right)^3 + \cdots$$
$$+\left[B_e - \alpha_e\left(v+\tfrac{1}{2}\right) + \gamma_e\left(v+\tfrac{1}{2}\right)^2 + \cdots\right]N(N+1)$$
$$-\left[D_e + \beta_e\left(v+\tfrac{1}{2}\right)^1 + \cdots\right][N(N+1)]^2 + \cdots \qquad [63]$$

The connection between these may not be readily apparent and so some of the values for the Y_{lj}'s will be given along with their connection to the band spectrum constants. One small intermediate step is that the power series of N(N+1) is converted to a power series in $(N + ½)^2$ by using the relationship $N^k(N+1)^k = [(N+½)^2-4]^k$ in order to make the coefficients simpler, and it should only affect the second order or higher terms, or terms of $\left[B_e/\omega_e\right]^2$ or higher in each of the coefficients.

$$Y_{00} = \frac{B_e}{8}\left(3a_2 - \frac{7}{4}a_1^2\right)$$

$$Y_{10} = \omega_e\left[1 + \left(\frac{B_e}{2\omega_e}\right)^2\left(25a_4 - \frac{95}{2}a_1a_3 - \frac{67}{4}{a_2}^2 + \frac{459}{8}{a_1}^2a_2 - \frac{1155}{64}{a_1}^4\right)\right]$$

$$Y_{20} = \frac{B_e}{2}\left[3\left(a_2 - \frac{5}{4}{a_1}^2\right) + \frac{1}{2}\left(\frac{B_e}{\omega_e}\right)^2\left(245a_6 - \frac{1365}{2}a_1a_5 - \frac{855}{2}a_2a_4 - \frac{1085}{4}{a_3}^2 + \frac{8535}{8}{a_1}^2a_4 + \frac{1707}{8}{a_2}^3 + \frac{7335}{4}a_1a_2a_3 - \frac{23865}{16}{a_1}^3a_3 - \frac{62013}{32}{a_1}^2{a_2}^2 + \frac{239985}{128}{a_1}^4a_2 - \frac{209055}{512}{a_1}^6\right)\right] \qquad [64]$$

$$Y_{01} = B_e\left[1 + \frac{1}{2}\left(\frac{B_e}{\omega_e}\right)^2\left(15 + 14a_1 - 9a_3 - 23a_1\,a_2 + \frac{21}{2}({a_1}^2 + {a_1}^3)\right)\right]$$

The other coefficients are found similarly and are connected to the band spectrum constants as follows.

$$\begin{aligned} Y_{10} &\sim \omega_e \\ Y_{20} &\sim -\omega_e x \\ Y_{30} &\sim \omega_e y \\ Y_{01} &\sim B_e \\ Y_{11} &\sim -\alpha_e \\ Y_{21} &\sim \gamma_e \\ Y_{02} &\sim -D_e \\ Y_{10} &\sim -\beta_e \end{aligned} \qquad [65]$$

The values for the Y_{lj}'s can be found experimentally and therefore in principle the adiabatic potential can be determined as long as the separation distance does not become so large that the rotational energy approaches that of the dissociation energy of the molecule. The most important "take away" from all of these equations is to note that the Y_{lj}'s are not exactly equal to the coefficients found using the Bohr theory. See for example the value for Y_{10}, which is the leading coefficient of $\left(v + \frac{1}{2}\right)$. It is not equal to ω_e but it differs from it

by a factor of the ratio $\left(\frac{B_e}{\omega_e}\right)^2$. Also Y_{01} is not the same as B_e but differs from it by small terms. This ratio is typically small for many molecules, typically of magnitude 10^{-6} so that for most practical purposes the first term is adequate to determine the energy of the rotational level. Some of the less massive molecules however, have values for the ratio in magnitude ~10^{-3}, for instance the H_2 molecule, which means higher terms in many of the Y_{lj}'s must be taken into consideration. The fact that the perturbation is larger for lighter molecules than heavy ones should follow from intuition of the model; a "heavy" rotor is obviously going to be more "rigid" than say a "light" rotor much like a heavy spring will also be more "rigid" in the sense that it will be difficult to stretch as compared to a lighter one. Another major "take away" from this derivation is the relationship of the energy level equation to the nuclear mass. Many spectra will change according to isotopic content and one can derive how the Y_{lj}'s will change as a function of the mass which then further assists in experimentally identifying isotopic mixtures from the rotation of molecules.

These calculations provide a means of determining the energy of the rotational levels from the experimental data tables generated from several workers. Herzberg provides a generous amount of information for diatomic molecules [77]. Knowledge of the energies of the rotational levels leads to an insight into the rotational temperature which can be attributed to the equilibrium temperature provided another source is not interfering with the local thermodynamic equilibrium. A finite time for a system to reach equilibrium

doesn’t mean it will always reach it. Many experiments have been found to have a finite equilibration time but the equilibrium is never observed due to other processes that introduce a quasi-equilibrium state to the system. Metastable transfer to molecules can lead to a hotter temperature since the rotation time of the molecule or the relaxation time can be longer than the lifetime of the states therefore allowing for “hot” molecules due to metastable transfer to lose their energy radiatively in the spectra that is being used for investigation of thermal equilibrium. The hot molecules are molecules populating higher states than would normally be populated by molecules following the thermal equilibrium condition. Hot molecules would then behave as if the populated states have been thermalized with a hotter temperature. Hot temperatures in a rotational spectrum would result in peaks in the envelope of the spectral peaks instead of a decaying exponential envelope that very low temperatures would exhibit. This is indeed the case for the jet under investigation in this work as shown in figure (3.7). The reason this phenomenon was unexpected to be not a major contribution is because of the low temperatures involved and that the processes of exciting the molecules should all start at the ground state of the molecule. This work shows that metastable helium delivers enough energy and that nitrogen has long enough lifetimes in excited states that the temperature measurement using this method of peak intensities and prior knowledge of the peak energies is not a viable thermometer. Still it can be by using a more complicated method.

5. CONCLUSION

The luminescence from trace gas atoms and molecules stimulated by metastable helium has proved to be a fertile ground for research. Many interactions seen even in a constricted environment as in this experiment are still yet to be fully understood, such as the role of non-radiative transitions due to long lived auto-ionizing states as compared to collision rates that play a role in the metastable transfer during collisions between helium and trace amounts of oxygen. Utilizing the Stark shift to change the overlap of oxygen and helium adsorption and emission curves could be enough to make this hypothesis conclusive. In the current experiment this should prove to be as easy as inserting electrodes and applying a linear DC field near the jet and liquid helium surface. Studies at these temperatures of the interplay between metastable helium and trace oxygen are not many and this work should help to inspire future works follow in its footsteps. Steering the jet could also be a future possibility in improving the ability of isolating processes at the liquid helium surface. Interacting multiple jets of different excited gases could also prove to be an interesting proposal for future work.

Nitrogen rotational spectra in the visual range, specifically the P_{12} branch of the first positive system, can be used as an upper bound of the temperature of a non-thermalized gas. The first positive system is a good thermometer for low density gases but it is shown that the requirements for thermal equilibrium in the

jet after leaving the discharge are not met. Although the method to correct the temperature from the hot molecule contribution involves photo-absorption techniques not available to the current experimental setup it could be done in future experiments through modifications that in design seem simple but in application may prove to be very lengthy and costly.

Can the higher energy levels of oxygen involved after the collision with metastable helium be used as a laser? Maybe, the measured intensity from the inferred flux of atoms definitely implies a large enough value for the gain per pass coefficient. If lasing action can be observed then a wealth of knowledge of what is happening in the active medium can be inferred using techniques already used in laser applications. The future is bright for the next explorers.

REFERENCES

[1] E. B. Gordon, et. al., "Stabilitzation of nitrogen atoms in superfluid helium," *JETP Lett.*, vol. 19, pp. 63-65, 1974.

[2] W. Siemens, "Ueber die elektrostatische Induction und die Verzögerung des Stroms in Flaschendrähten," *Poggendorf's Annalen Der Physik*, vol. 178, pp. 66-122, 1857.

[3] J. C. Maxwell, "On Physical Lines of Force," *The London, Edinburgh, and Dublin Philosophical Magazine and Journal of Science*, vol. 4, pp. 161-175, 1861.

[4] J. C. Maxwell, "A dynamical theory of the electromagnetic field," *Philosophical Transactions of the Royal Society of London*, vol. 155, pp. 459-512, 1865.

[5] M. K. E. L. Planck, "Über eine Verbesserung der Wienschen Spektralgleichung," *Verhandlungen der Deutschen Physikalischen Gesellschaft*, vol. 2, pp. 202-204, 1900.

[6] A. Einstein, "Strahlungs-emission und -absorption nach der Quantentheorie," *Verhandlungen der Deutschen Physikalischen Gesellschaft*, vol. 18, pp. 318-323, 1916.

[7] R. Ladenburg and H. Kopfermann, "Experimental Proof of 'Negative Dispersion'," *Nature*, vol. 122, pp. 438-439, 1928.

[8] G. N. Lewis, "The conservation of photons," *Nature*, vol. 118, pp. 874-875, 1926.

[9] C. J. Humphreys, T. L. deBruin, and W. F. Meggers, "Regularities in the second spectrum of xenon," *Bureau of Standards Journal of Research*, vol. 6, p. 287, 1931.

[10] J. C. Maxwell, "On Boltzmann's theorem on the average distribution of energy in a system of material points," *Trans. Cambridge Phil. Soc.*, vol. 12,

pp. 547-570, 1879.

[11] L. E. Boltzmann, "Referat über die Abhandlung von J.C. Maxwell: “Über Boltzmann's Theorem betreffend die mittlere verteilung der lebendige Kraft in einem System materieller Punkte”," *Wied. Ann. Beiblätter*, vol. 5, pp. 403-417, 1881.

[12] M. W. Zemansky, *Heat and Thermodynamics, 4th ed.* New York: McGraw-Hill, 1957.

[13] R. C. Retherford W. E. Lamb, "Fine Structure of the Hydrogen Atom by a Microwave Method," *Phys. Rev.*, vol. 72, pp. 241-243, 1947.

[14] C. H. Townes, *How the Laser Happened: Adventures of a Scientist*. New York: Oxford University Press, 2002.

[15] B. Kröger, *Hermann Haken: From the Laser to Synergetics: A Scientific Biography of the Early Years*. New York: Springer, 2015.

[16] T. H. Maiman, "Stimulated Optical Radiation in Ruby," *Nature*, vol. 187, pp. 493-494, 1960.

[17] W. R. Bennett Jr., D.R. Herriott, and A. Javan, "Population Inversion and Continuous Optical Maser Oscillation in a Gas Discharge Containing a He-Ne Mixture," *Physical Review Letters*, vol. 6, p. 106, 1961.

[18] C. K. N. Patel, "Continuous-Wave Laser Action on Vibrational-Rotational Transitions of CO2," *Physical Review*, vol. 136, pp. A1187-A1193, 1964.

[19] E. Hecht, *Optics, 4th ed.* Boston: Addison-Wesley, 2001.

[20] S. N. Bose, "Plancks Gesetz und Lichtquantenhypothese," *Zeitschrift für Physik*, vol. 26, pp. 178-181, 1924.

[21] B. P. Abbott, et. al., "Observation of Gravitational Waves from a Binary Black Hole Merger," *Physical Review Letters*, vol. 116, p. 061102, 2016.

[22] A. Einstein, "Über einen die Erzeugung und Verwandlung des Lichtes betreffenden heuristischen Gesichtspunkt," *Annalen der Physik*, vol. 322,

pp. 132-148, 1905.

[23] Louis de Broglie, "Recherches sur la théorie des quanta (Researches on the quantum theory), Thesis, Paris 1924," *Ann. de Physique*, vol. 3, p. 22, 1925.

[24] C. Davisson and L. H. Germer, "Diffraction of Electrons by a Crystal of Nickel," *Physical Review*, vol. 30, p. 705, 1927.

[25] O. Stern, "Beugung von Molekularstrahlen am Gitter einer Krystallspaltfläche," *Naturwissenschaften*, vol. 17, no. 21, p. 391, 1929.

[26] F. Knauer and O. Stern, "über die Reflexion von Molekularstrahlen," *Zeitschrift für Physik*, vol. 53, p. 779, 1929.

[27] V. S. Letokhov and V. I. Balykin, *Atom Optics with Laser Light, Laser Science and Technology: An International Handbook*, C.V. Shank, Y.R. Shen, and H. Walther V.S. Letokhov, Ed.: Harwood Academic, 1995, vol. 18.

[28] P. Berman, *Atom Inferferometry*. New York: Academic Press, 1997.

[29] J. M. Hogan, M. A. Kasevich, S. Rajendran, and P. W. Graham, "New Method for Gravitational Wave Detection with Atomic Sensors," *Physical Review Letters*, vol. 110, p. 171102, 2013.

[30] K. G. H. Baldwin, "Metastable helium: atom optics with nano-grenades," *Contemporary physics*, vol. 46, pp. 105-120, 2005.

[31] I. N. Krushinskaya, R. Boltnev, I.B. Bykhato, A. A. Pelmenev, D. M. Lee, and V. V. Khmelenko, "Dynamics of thermoluminescence spectra of impurity-helium condensates containing stabilized nitrogen and oxygen atoms," *Journal of Low Temperature Physics*, vol. 38, pp. 833-871, 2012.

[32] H.-D. Denner and G. Klipping, "The thermo-mechanical effect of superfluid helium and its technical application," in *Proceedings of the 1989 Cryogenic Engineering Conference*, New York, 1990.

[33] L. Landau, "On the theory of Superfluidity," *Physical Review*, vol. 75, p. 884, 1949.

[34] L. Tisza, "On the theory of superfluidity," *Physical Review*, vol. 75, p. 885, 1949.

[35] K. Mendelssohn and J. G. Daunt, "Film Transfer in Helium II: I - The Thermo-Mechanical Effect," in *Proceedings of the Physical Society Section A*, vol. 63, 2002, p. 1305.

[36] F. London, "The electromagnetic equations of the supraconductor," *Proceedings fo the Royal Society A: Mathematical, Physical and Engineering Sciences*, vol. 149, p. 866, 1935.

[37] R. Skalak and S. P. Sutera, "The history of Poiseuille's Law," *Annual Review of Fluid Mechanics*, vol. 25, p. 1, 1993.

[38] J. E. Hirsch, "Kinetic Energy Driven Superconductivity and Superfluidity," *Modern Physics Letters B*, vol. 25, p. 2219, 2011.

[39] E. B. Gordon, L. P. Mezhov-Deglin, 0. F. Pugachev, and V. V. Khmelenko, "Thermal stability of condensed systems that contain trapped atoms," *Sov. Phys. Journal of Experimental and Theoretical Physics*, vol. 19, p. 63, 1974.

[40] H. Kunttu, D. M. Lee, and V. V. Khmelenko, "Recent Progress in Studies of Nanostructured Impurity-Helium Solids," *Journal of Low Temperature Physics*, vol. 148, pp. 1-31, 2007.

[41] S. Mao, A. Meraki, S. C. Wilde, P. T. McColgan, A. A. Pelmenev, R. E. Boltnev, D. M. Lee and V. V. Khmelenko, "Application of cold beam of atoms and molecules for studying luminescence of oxygen atoms," *Journal of Physics: Conference Series*, vol. 568, p. 032010, 2014.

[42] J. Ahokas, J. Eloranta, H. Kunttu, and E. A. Popov, "Generation of intrinsic excitations in superfluid 4He by using gas jet approach," *Journal of Low Temperature Physics*, vol. 138, pp. 85-90, 2005.

[43] John Doyle et al., "Buffer gas loading into a magnetic trap," *Phys. Rev. A*, vol. 52, no. 4, pp. R2515-R2518, 1995.

[44] I. Langmuir, "The constitution and fundamental properties of solids and liquids," *Journal of the American Chemical Society*, vol. 38, p. 2221, 1916.

[45] E. Jehin, D. Hutsemekers, J. Manfroid, and A. Decock, "Forbidden oxygen lines in comets at various heliocentric distances," *Astronomy & Astrophysics*, vol. 555, pp. 1-15, 2013.

[46] D. W. Ernie and H. J. Oskam, "Energy transfer between helium metastable particles and neon," *Physical Review A*, vol. 21, pp. 95-100, 1980.

[47] G. Meyers and A. J. Cunningham, "Rate measurements of reactions of helium metastable species at atmospheric pressures. II. He2 (2 3Σ+ u) in pure afterglows," *Journal of Chemical Physics*, vol. 67, p. 1942, 1977.

[48] A. V. Phelps, *Third International Conference on Ionization Phenomena in Gases, Venice*. Milan: Italian Society of Physics, 1957.

[49] C. B. Collins and F. W. Lee, "Measurement of the rate coefficients for the de-excitation reactions of He2 (3Σ u) metastables with Ne, Ar, N2, CO, CO2, and CH4," *Journal of Chemical Physics*, vol. 67, p. 2798, 1977.

[50] Theodor Förster, *Fluoreszenz organischer Verbindungen*. Göttingen: Vandenhoeck & Ruprecht, 1950.

[51] J. L. Bohn, "Inelastic collisions of ultracold polar molecules," *Physical Review A*, vol. 63, p. 052714, 2001.

[52] P. Emmott and R. E. Wilson, "The use of tesla-luminescence spectra for the determination of nitrogen in helium," *Talanta*, vol. 11, pp. 1011-1018, 1964.

[53] B. Zygelman, "Radiative deexcitation of singlet metastable helium by collisions with helium atoms," *Physical Review A*, vol. 43, pp. 575-577, 1991.

[54] M. G. Payne, et. al., "Kinetics of He(2S1) Using Resonance Ionization Spectroscopy," *Physical Review Letters*, vol. 35, pp. 1154-1156, 1975.

[55] R. Katano, Y. Isozumi, and S. Masaoka, "Analysis of outputs from a helium-filled proportional counter at liquid helium temperature," *Nuclear Instruments and Methods in Physics Research B*, vol. 179, pp. 133-144, 2001.

[56] J. A. Hornbeck and J. P. Molnar, "Mass Spectrometric Studies of Molecular

Ions in the Noble Gases," *Physical Review*, vol. 84, p. 621, 1951.

[57] T. D. Raymond, M. E. Riley, and A. V. Smith, "Measurement of select transition strengths and autoionizing lifetimes in atomic oxygen," *Physical Review A*, vol. 45, pp. 4688-4697, 1992.

[58] A Wirsing, M. Barthel, J. Plenge, E. Rühl, and R. Flesch, "Inner-valence photoionization of O(^1D): Experimental evidence for the 2s^22p^4(1D)→2s^12p^5(^1P) transition," *Journal of Chemical Physics*, vol. 128, p. 074307, 2008.

[59] V. V. Khmelenko, et al., "Luminescence of Oxygen Atoms Stimulated by Metastable Helium at Cryogenic Temperatures," *Physical Review Letters*, vol. 111, p. 183002, 2013.

[60] Q. Wei, I. Lyuksyutov, and D. Herschbach, "Merged-Beams for Slow Molecular Collision Experiments," *Journal of Chemical Physics*, vol. 137, p. 054202, 2012.

[61] V. Milosavljevic, A.R. Ellingboe, and S. Daniels, "Influence of plasma chemistry on oxygen triplets," *European Physical Journal D*, vol. 64, pp. 437-445, 2011.

[62] N. R. Hutzler, H. Lu, and J. M. Doyle, "The Buffer Gas Beam: An Intense, Cold, and Slow Source for Atoms and Molecules," *Chemical Reviews*, vol. 112, pp. 4803-4827, 2012.

[63] M. K. E. L. Planck, "Entropie und Temperatur strahlender Wärme," *Annalen der Physik*, vol. 306, no. 4, pp. 719-737, 1900.

[64] L. E. Boltzmann, "Weitere Studien über das Wärmegleichgewicht unter Gasmolekülen," *Sitzungsberichte Akademie der Wissenschaften*, vol. 66, pp. 275-370, 1872.

[65] T. Lin, et. al., "Nitrogen-doped mesoporous carbon of extraordinary capacitance for electrochemical energy storage," *Science*, vol. 350, no. 6267, pp. 1508-1513, 2015.

[66] C. Biloiu, X. Sun, Z. Harvey, and E. Scime, "Determination of rotational and vibrational temperatures of a nitrogen helicon plasma," *Review of Scientific*

Instruments, vol. 77, p. 10F117, 2006.

[67] S. M. Naude, "Quantum Analysis of the Rotational Structure of the First Positive Bands of Nitrogen," *Proceedings Royal Society London A: Mathematical, Physical and Engineering Sciences*, vol. 136, p. 114, 1932.

[68] C. Biloiu, X. Sun, Z. Harvey, and E. Scime, "An alternative method for gas temperature determination in nitrogen plasmas: Fits of the bands of the first positive system (B Π 3 g → A Σ 3 u +)," *Journal of Applied Physics*, vol. 101, p. 073303, 2007.

[69] H. Hönl and F. London, "Über die Intensitäten der Bandenlinien," *Zeitschrift für Physik*, vol. 33, pp. 803-809, 1925.

[70] L. Tonks and I. Langmuir, "A general theory of the plasma of an arc," *Physical Review*, vol. 34, p. 876, 1929.

[71] E. Schrödinger, "Quantisierung als Eigenwertproblem," *Annalen der Physik*, vol. 384, pp. 273-376, 1926.

[72] E. U. Condon and G. H. Shortley, "The Theory of Atomic Spectra," *Cambridge University Press*, 1935.

[73] M. Mizushima, "Perturbation Formulas," *Journal of Mathematical Physics*, vol. 12, p. 2216, 1971.

[74] H. Padé, "Sur la répresentation approchée d'une fonction par des fractions rationelles," *Annales scientifiques de l'École Normale Supérieure*, vol. 9, pp. 1-93, 1892.

[75] G. A. Baker and J. L. Gammel, *The Padé Approximants in Theoretical Physics*. New York: Academic Press, 1970.

[76] R. G. Littlejohn, "The Van Vleck Formula, Maslov Theory, and Phase Space Geometry.," *Journal of Statistical Physics*, vol. 68, pp. 7-50, 1992.

[77] G. Herzberg, *Molecular Spectra and Molecular Structure I: Spectra of Diatomic Molecules*. Princeton, New Jersey: D. Van Nostrand Company, Inc., 1950.

[78] J. L. Dunham, "The Energy Levels of a Rotating Vibrator," *Physical Review*, vol. 41, p. 721, 1932.

APPENDIX

BIOGRAPHICAL SKETCH

Scott Wilde was born in Riyadh, Saudia Arabia because his father was working in construction management of King Fahd airport at the time. He attended University of Nevada, Las Vegas (UNLV), where he received his Masters and Bachelor of Science degrees in physics. His work as an undergraduate involved simulations of the early universe with Dr. Stephen Lepp and his work outside of the university involved nuclear physics of neutron detection and remote sensing of fissile materials at the Nevada Test Site and also at the Remote Sensing Laboratory at Nellis Air Force Base with Drs. Warnick Kernan, Paul Guss, and Raymond Keegan. During which time he gave conference talks at American Nuclear Society's 2008 annual meeting and also at Los Alamos National Laboratory's "Laboratory Directed Research & Development" conference in 2009. While working on his Masters he paid his bills by starting his own business as a programming consultant which afforded him travel to Argonne National Laboratory's Advanced Photon Source, Lawrence Berkeley National Laboratory's Advanced Light Source for Dr. Clemens Heske, and Sandia National Laboratory for writing software packages to enable faster data analysis methods and automated research for the many researchers buried in their work. For his Masters he studied nonlinear optics and developed a passion to understand electron orbitals in atoms and eventually molecules after his first taste of graduate level electrodynamics and his time spent in the lab with

his advisor Dr. David Shelton. He began doctoral studies at Texas A&M University in 2011 by working with Dr. Marlan Scully's group, the Institute for Quantum Science and Engineering, and first worked on theoretical materials for solar energy capture until 2012 when he started working in the low temperature physics laboratory with his future research advisor Dr. David M. Lee studying nonlinear spin dynamics and optical spectra from impurity helium solids. He became intensely interested in the details of the dynamics of the cold helium jets that were being used by Lee's group to create impurity helium solids and pursued a complete understanding of the luminescence of these jets for his doctoral research.

The following publications were a result of work conducted during his doctoral study.

D. L. Hawthorne, S. Wilde, D.M. Lee, "Simulations of Non-linear Spin Dynamics in Spin Polarized Dilute 3He-4He Mixtures," Journal of Low Temperature Physics Vol. **171**, p165. (2013)

V. V. Khlemenko, S. Mao, A. Meraki, S.C. Wilde, P. McColgan, A. A. Pelmenev, R. E. Boltnev, and D. M. Lee, "Luminescence of oxygen atoms stimulated by metastable helium at cryogenic temperatures," Physical Review Letters, **111**, 183002 (2013)

V. V. Khmelenko, S. Mao, A. Meraki, S. C. Wilde, P. T. McColgan, A. A. Pelmenev, R. E. Boltnev, and D. M. Lee, "Application of cold beam of atoms and molecules for studying luminescence of Oxygen atoms stimulated by metastable

helium,” *27th International Conference on Low Temperature Physics*, published in *Journal of Physics: Conference Series* **568**, 032010, (2014)

R. E. Boltnev, I. B. Bykhalo, I. N. Krushinskaya, A. A. Pelmenev, V. V. Khmelenko, S. Mao, A. Meraki, S. C. Wilde, P. T. McColgan, “Optical and spin resonance studies of Xenon-Nitrogen-Helium condensates containing Nitrogen and Oxygen atoms.” *The Journal of Physical Chemistry, A,* **119**, 2438-2448 (2015)